Journal of Advanced Research xxx (xxxx) xxx

Contents lists available at ScienceDirect

Journal of Advanced Research

journal homepage: www.elsevier.com/locate/jare

Original Manuscript

Dietary EGCG reshapes metabolic-epigenetic interplay to induce transgenerational host defense

Wenqi Huang [b,1], Shiye Lin [a,b,1], Xuanyu Zheng [c], Mohamed A. Farag [d], Thomas Efferth [e], Jesus Simal-Gandara [b], Zimiao Chen [f,*], Jianbo Xiao [a,b,g,**], Hui Cao [b,*]

[a] State Key Laboratory for Development and Utilization of Forest Food Resources, Zhejiang A&F University, Hangzhou 311300, China
[b] Universidade de Vigo, Nutrition and Bromatology Group, Department of Analytical Chemistry and Food Science, Instituto de Agroecoloxía eAlimentación (IAA)-CITEXVI, 36310 Vigo, Spain
[c] College of Life Science and Technology, Jinan University, 510632 Guangzhou, China
[d] Pharmacognosy Department, Faculty of Pharmacy, Cairo University, Cairo 11562, Egypt
[e] Department of Pharmaceutical Biology, Institute of Pharmaceutical and Biomedical Sciences, Johannes Gutenberg University, 55128 Mainz, Germany
[f] The First Affiliated Hospital of Wenzhou Medical University, Wenzhou, China
[g] Research Group on Food, Nutritional Biochemistry and Health, Universidad Europea del Atlántico, Isabel Torres 21, 39011 Santander, Spain

HIGHLIGHTS

- EGCG induces transgenerational host defense in mice and *Drosophila melanogaster*.
- EGCG activates glycolysis to reshape metabolic programming and support anabolism in *Drosophila*.
- EGCG increases H3K27ac level in offspring, thereby mediating the enhanced host defense.
- EGCG reduces intestinal amino acids (in particular tyrosine) to trigger the integrated stress response.
- Ovary-derived lactate may serve as a substrate for the increased H3K27ac in offspring.

GRAPHICAL ABSTRACT

Our mouse studies were approved by the Experimental Animal Science Ethics and Welfare Committee of Jinan University, China (IACUC-20231030-03). Experiments were performed according to the guidelines for the Care and Use of Experimental Animals of Jinan University.

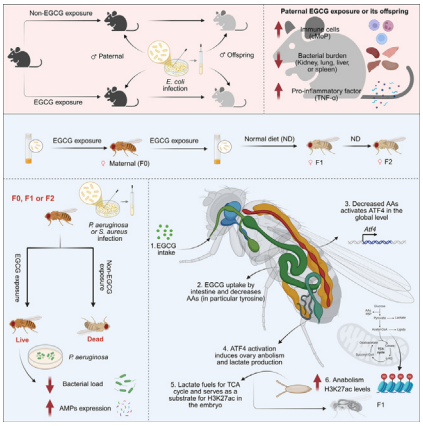

ARTICLE INFO

Article history:
Received 4 November 2025
Revised 29 March 2026
Accepted 11 April 2026
Available online xxxx

ABSTRACT

Introduction: Parental diet is a key determinant of offspring health and immune function, in part through epigenetic regulation. Metabolic and epigenetic networks integrate nutrient sensing with chromatin dynamics to maintain cellular and organismal homeostasis. However, the mechanism by which specific dietary bioactive compounds reshape metabolic-epigenetic networks to drive transgenerational adaptive responses remains poorly understood.

* Corresponding authors.
** Corresponding author at: State Key Laboratory for Development and Utilization of Forest Food Resources, Zhejiang A&F University, Hangzhou 311300, China.
E-mail addresses: huangwenqi1997@outlook.com (W. Huang), linshiye33@163.com (S. Lin), zxy78876@163.com (X. Zheng), mohamed.farag@pharma.cu.edu.eg (M.A. Farag), efferth@uni-mainz.de (T. Efferth), jsimal@uvigo.gal (J. Simal-Gandara), zimiaochen@163.com (Z. Chen), jianboxiao@uvigo.es (J. Xiao), hui.cao@uvigo.es (H. Cao).
[1] These authors equally contributed.

https://doi.org/10.1016/j.jare.2026.04.028

Please cite this article as: W. Huang, S. Lin, X. Zheng et al., Dietary EGCG reshapes metabolic-epigenetic interplay to induce transgenerational host defense, Journal of Advanced Research, https://doi.org/10.1016/j.jare.2026.04.028

Keywords:
Epigenetics
Flavonoids
Histone acetylation
Host defense
Metabolic reprogramming
Phytotherapy
Transgenerational inheritance

Objectives: Here, we investigate whether and how epigallocatechin-3-gallate (EGCG), a well-characterized dietary bioactive compound, modulates heritable host defense through metabolic-epigenetic crosstalk.

Methods: To address both physiological relevance and mechanistic insight, we employed mouse and *Drosophila melanogaster* models. Parental animals were administered EGCG, and offspring were subsequently assessed for immune function upon infection with *Escherichia coli*, *Pseudomonas aeruginosa*, or *Staphylococcus aureus*. By integrating transcriptomics, metabolite analysis, and isotopic tracing, we analyzed metabolism-related pathways and constructed a dynamic network linking metabolic changes to epigenetic modifications in *Drosophila*.

Results: In mice, EGCG administration led to a decrease in *Escherichia coli* burden across multiple tissues in paternal and male offspring in a sex-specific manner, accompanied by metabolic and pro-inflammatory factor changes. In *Drosophila melanogaster*, early-life EGCG exposure increased survival upon *Pseudomonas aeruginosa* or *Staphylococcus aureus* infection and persisted for two subsequent generations. Mechanistically, EGCG reduced intestinal amino acids, thereby moderately inducing activation of activating transcription factor 4 (ATF4), which in turn enhanced maternal glycolysis and immune adaptation. Tyrosine supplementation abolished the enhanced host defense and metabolic changes. Furthermore, ATF4-induced activation of glycolysis promoted ovarian lactate production, serving as a substrate for increased global H3K27 acetylation in the offspring.

Conclusion: Together, these findings suggest that dietary bioactive compounds modulate metabolic and gene regulatory processes, with functional evidence supporting a role for amino acid metabolism and lactate in linking metabolic remodeling to enhanced resistance to infection in the offspring. This work provides mechanistic insight into how diet can shape heritable immune function through metabolic-epigenetic interplay.

Introduction

Immune adaptation enables organisms to adjust host defense in response to environmental cues, thereby maintaining fitness without permanent genetic change [1]. This plastic strategy involves the reprogramming of cellular metabolism and epigenetic modifications, and may be transmitted to subsequent generations [2]. Consistent with this notion, transgenerational inheritance of immune traits in response to parental environmental stimuli has been documented in multiple species [3].

Dietary factors are a critical environmental signal that induces metabolic adaptation of immune cells. For instance, dietary restriction can profoundly enhance the host defense and survivorship after infection by increasing the anti-microbial peptides [4]. Many core metabolites such as ATP, S-adenosyl methionine, acetyl-CoA, NAD/NADP and α-ketoglutarate are essential substrates for chromatin modifiers [5]. Dietary stimuli modulate core metabolites to regulate the epigenome *via* nutrient-sensing pathways such as mTOR and AMPK [6,7]. Metabolic regulation in germline cells is closely linked to epigenetic regulation, and thereby may affect immune phenotype changes in offspring.

Among dietary bioactive compounds, epigallocatechin gallate (EGCG), a major polyphenol in green tea, has emerged as a potent modulator of host metabolism and immune function [8]. EGCG has been shown to influence key metabolic pathways, including lipid metabolism, mitochondrial activity, and insulin/TOR signaling [9,10]. In addition, many epigenetic-related enzymes such as histone acetyltransferases, deacetylases, and DNA methyltransferases can also be regulated by EGCG [11]. These results imply that dietary EGCG may function as potent stimuli to induce metabolic-epigenetic reprogramming in immune cells. However, whether dietary EGCG can induce heritable immune adaptation and enhance host defense across generations remains largely unknown.

Herein, we explore whether dietary EGCG can induce transgenerational host defense against infections using mice and *Drosophila melanogaster* models. Combined with isotopic tracing analysis, we show that parental EGCG exposure effectively increases the resistance to bacterial infections across generations by reshaping metabolic-epigenetic interplay. These results support the idea that dietary bioactive compounds can induce transgenerational immune adaptation and highlight the importance of parental dietary bioactive compounds in shaping health outcomes in adult offspring.

Methods

Mouse models

Our mouse studies were approved by the Experimental Animal Science Ethics and Welfare Committee of Jinan University, China (IACUC-20231030-03). Experiments were performed according to the guidelines for the Care and Use of Experimental Animals of Jinan University. The C57BL/6J mice obtained from Veiton Lihua Co., Ltd. (Beijing, China) were kept on a 24-h 12 h-12 h light–dark cycle at 18–25 °C and received rodent chow from Synergy Bio Co., Ltd. (catalog no. XTCON50J; standard diet containing 20% protein, 70% carbohydrates, and 10% fat) and free access to water. After acclimatization for seven days, twenty-five 5-week-old male mice were intragastrically fed with PBS solution (F0 control) and 300 mg/kg EGCG [12] dissolved in PBS solution (F0 EGCG-exposed). The EGCG dose (300 mg/kg) was selected based on previous studies and is below levels reported to induce genotoxicity or hepatotoxicity [13,14].

Six weeks later, F0 control and F0 EGCG-exposed mice were mated with healthy naive females at a ratio of 1:2. The first generation (F1 control and F1 EGCG-exposed) was used for further experiments after nine to ten weeks of rodent chow. The body weight and food intake were measured weekly.

E. coli infection and bacterial burden in mice

E. coli was grown on a liquid Luria-Bertani (LB) medium at 37 °C. *E. coli* was centrifuged (4 °C, 6,500 g for 3 min), washed by PBS and counted using a hematocytometer. First-generation offspring (F1 control and EGCG-exposed mice) and residual F0 mice (control and EGCG-exposed) were subjected to an intraperitoneal injection (i.p.) with a dose of 1×10^5 CFUs of *E. coli*. Kidney, lung, liver, and spleen were washed using PBS and collected at 12 h and 36 h post

infection. Samples were homogenized by PBS at a ratio of 1:9 (*w/v*), and the homogenates were then serially diluted with sterile PBS from 10^1 to 10^4 times, and plated on LB agar plates, and incubated overnight at 37 °C [15]. The bacterial colonies were counted the next day.

Serum cytokines detection and flow cytometry analysis in mice

Mice were anesthetized with 2% isoflurane. Blood was collected by eye plucking and serum samples were separated by centrifugation (4 °C, 3000 rpm, 30 min) at 0 h, 4 h, and 36 h after infection. Then, the serum TNF-α and IL-6 levels were determined using ELISA kits (Solarbio; catalog no. SEKM-0034 and SEKM-0007), according to the manufacturer's guidelines. Bone marrow cells were harvested and flushed by PBS from the tibia of one leg 36 h after infection. The samples were incubated overnight in the dark at 4 °C with 3 μL of each anti-mouse CD11b (TONBO; catalog no. 75-0112-U100), Ly-6G (Invitrogen; catalog no. 61-9668-82), Ly-6C (Invitrogen; catalog no. 25-5932-8), I-A/I-E (MHC class II; biolegend; catalog no.107608), CD11c (TONBO; catalog no. 20-0114-U100). The remaining pellet was resuspended in 150 μL PBS. Peripheral bone marrow progenitor cells ($CD11b^+$), monocytes (Ly6Chigh), macrophages (F4/80high), neutrophils ($Ly6G^+$), and dendritic cells ($CD11B^+MHCII^+CD11C^+$) were separated and analyzed by flow cytometry. Data were analyzed using FlowJo 10.7.1 (FlowJo LLC).

Serum glucose and triglycerides measurements in mice

Serum samples were collected as described in *4.3*. The levels of serum glucose and triglyceride were determined using kits according to the manufacturer's guidelines from Nanjing Jiancheng Bioengineering Institute (catalog no. F006-1-1 and A110-1-1). In brief, 10 μL of serum samples were diluted with saline (0.9% NaCl) and transferred into glucose or triglyceride reagent. The reaction mixture was shaken and incubated at 37 °C for 10 min. The absorbance was measured at 505 nm (glucose) or 500 nm (triglyceride) using a microplate reader. A standard curve with solutions of known concentrations of glucose or triglyceride was constructed.

Drosophila models

Wild-type male and/or female fruit fly *Drosophila melanogaster* Oregon-R strains were utilized in all assays and sourced from Carolina Biological Supply Company (Burlington, NC, USA). The flies were maintained under standardized conditions, a temperature of 25 °C and relative humidity of 60%, with a 12-h light–dark photoperiod. Flies were collected as experimental within 12 h post-eclosion (labeled as 0 days old). Each of vial diet was replaced with fresh provisions every 2–3 days. The recipe of normal yeast-based diet (Control) contained 6.5% corn meal, 4% sucrose, 0.8% agar and 1% dry yeast. For EGCG-rich food preparation, purified EGCG powder was dissolved in water and sterilized by filtration with 0.22 μM membrane. A 50 mM of EGCG stock solution was supplemented to the normal yeast-based diet to a final concentration of 2 and 10 mM when the temperature decreased to 50–60 °C [16,17]. For adulthood treatment, 2–3 days old flies were randomly placed on Control or EGCG-rich food for 6 days. For embryonic exposure, male and female flies were allowed to mate for 3 days under the Control or EGCG-rich food, adult female flies were collected and maintained on the same diets.

For curcumin or rapamycin treatment [4], 40 μL of curcumin (10 mM and 50 mM) or 12.5 mM rapamycin (MedChemExpress; catalog no. HY-10219) was dissolved in ethanol and aliquoted onto the surface of 10 mL food in a standard wide vial. Ethanol was used as a vehicle for both. Treated food was evaporated under a fume hood for 2–4 h until dryness. For metformin (MedChemExpress; catalog no. HY-B0627) and amino acids treatment [18], 10 mM metformin, and amino acids (valine, leucine, isoleucine, methionine, phenylalanine, and tyrosine) were supplemented to the normal yeast-based diet. For sodium oxamate (MedChemExpress; catalog no. HY-W013032A) treatment, 10 mM or 50 mM sodium oxamate of powder was supplemented to the 10 mM EGCG-rich diet. Five adult flies were pooled for measuring body weight for one sample.

Survival and bacterial burden assays in flies

Bacterial infection and measurement of survival rates were performed as described previously [4]. In brief, *P. aeruginosa* or *S. aureus* was grown on a liquid LB medium at 37 °C. The bacterial dose was adjusted to an OD_{600} value of 1.0 or 10–25 by resuspending in liquid LB, respectively. The bacterial culture was kept on ice during infection. After each infection, flies were placed in a vial with the normal yeast-based diet and then entrained under 12 h light/12 h dark cycles at 25 °C for two to three days. Marginal survival probabilities from several replicate experiments were calculated, and significance values were obtained using survival analysis assays [19]. For bacterial burden assay, at 6 h after *P. aeruginosa* infection, 5 flies were pooled and homogenized by 1 mL sterile PBS. Fly extract (50 μL) was plated onto the LB agar plate and incubated at 37 °C for 6–8 h. The visible colonies were counted using a hematocytometer.

Lifespan assessment

Adult flies were collected within 8 h after eclosion and sorted under CO_2 anesthesia. For F0 generation, female flies were fed normal yeast-based diet or EGCG-rich diet for 6 days, and 20 individuals were randomly allocated to each vial with a normal yeast-based diet. For F1 generation, 20 female flies were randomly assigned to each vial with a normal yeast-based diet. Throughout the experiment, flies were maintained at 25 °C under 60% humidity and a 12-h light:12-h dark cycle, and transferred to fresh vials every 3 to 4 days. Mortality was monitored by checking for dead flies in the vials and recording the number of deaths.

Fecundity analysis

At two days after eclosion, 15 female flies and 15 male flies were collectively transferred to the normal yeast-based diet or EGCG-rich diet, flies were transferred to fresh vials every three days. Six days after dietary manipulation, anesthetized flies were separated into groups of three males with three females. After 24 h, the egg number in each vial was counted.

Imaging analysis

To analyze ovary size, dissected ovaries were placed in phosphate-buffered saline (PBS) on a silicone pad. Images were captured using a fluorescence stereomicroscope (Nikon stereo microscope, SMZ25). The area of the ovary from the top view was measured using the Image J software (version 1.53, NIH, Bethesda, MD, USA).

Glucose and triglyceride measurements in flies

For glucose measurement, flies were pooled and weighed in groups of 30, each sample was homogenized in 300 μL distilled H_2O. The homogenates were centrifuged at 4 °C, 8,000 *g* for 15 min and the supernatant was transferred into glucose reagent (Biorbpt; catalog no. orb390731). The reaction mixture was incu-

bated at 37 °C for 10 min. The absorbance at 505 nm was then measured using a microplate reader and glucose content was calculated by comparison with a standard curve constructed with solutions of known concentrations of glucose (Biorbpt; catalog no. orb390731). For triglyceride measurement, 30 flies were homogenized in 300 μL heptane/isopropanol (*v*/*v*/ = 3.5/6.5). The homogenates were centrifuged at 4 °C, 10,000 *g* for 15 min and the supernatant was transferred into Triglyceride Reagent (Biorbpt; catalog no. orb390792). The reaction mixture was kept on ice and the absorbance at 500 nm was then measured using a microplate reader. A standard curve was also constructed with solutions of known concentrations of triglyceride (Biorbpt; catalog no. orb390792). Glucose and triglyceride levels are expressed as glucose/fly weight or triglyceride/fly weight.

Stable isotope labelling

Adult female flies were starved for 4 h before experiments. Following a 24-h or 48-h feeding regimen with 10% U-^{13}C6-glucose (Sigma-Aldrich, catalog no. 310808) dissolved in PBS and soaked in a filter paper. Twenty fat bodies or 10 whole bodies were collected and pooled into each tube for subsequent GC–MS or LC-MS analysis [20].

GC–MS analysis

For metabolite extraction, individual sample was prepared by pooling 200–400 eggs, 20 individual tissues (fat bodies, ovaries, or guts), or 5 whole bodies, respectively. Hemolymph was collected and pooled from 10 flies by centrifugation (4 °C, 5,000 g, 10 min) with a spin column. Samples were collected under light CO_2 anesthesia and rapidly frozen in −80 °C fridge. The samples were suspended with 1 mL of acetonitrile/methanol/H_2O (*v*/*v*/*v* = 2:2:1) containing 20 μM internal standards (L-norvaline) to precipitate the proteins. The frozen tissues or whole bodies were ground using a homogenizer and stored at −20 °C for 2 h. The hemolymph was subjected to three freeze–thaw cycles at −80 °C. After centrifugation at 4 °C and 14,000 *g* for 15 min, the supernatant was transferred to a new Eppendorf tube and dried in a vacuum concentrator at 37 °C. The dry pellets were reconstituted into 50 μL dimethylformamide first and then derivatized with 75 mL N-methyl-N-(tertbutyldimethylsilyl) trifluoroacetamide (MTBSTFA) + 1% tertbutyldimetheylchlorosilane (TBDMCS) and incubated at 60 °C for 30 min. Samples were analyzed using a Trace 1300 gas chromatography (GC) coupled to an ISQ 7000 single quadruple analyzer (Thermo Fisher, Massachusetts, USA). A Rxi-5 ms capillary column (30 m, 250 μm, and 0.25 μm film thickness) was used. The GC oven program was set as follows: Initially, 110 °C for 4 min, 15 °C /min up to 215 °C, followed by 5 °C /min up to 260 °C, and finally at 25 °C /min up to 310 °C for 3 min. The flow rate was maintained at 1.5 mL/min, and helium was used as a carrier gas during the analysis. The temperatures of the inlet and GC–MS interface temperatures were maintained at 300 and 230 °C, respectively. For targeted metabolomics, SIM mode was used and the following metabolites were detected as TBDMS derivatives: GAP (*m*/*z* 383), G3P (*m*/*z* 571), 3PG (*m*/*z* 585), PEP (*m*/*z* 453), pyruvate (*m*/*z* 259), lactate (*m*/*z* 233 and 261), glutamine (*m*/*z* 357 and 431), citrate (*m*/*z* 431 and 459), α-ketoglutarate (*m*/*z* 346), succinate (*m*/*z* 289), fumarate (*m*/*z* 287), malate (*m*/*z* 391 and 419), glutamate (*m*/*z* 330 and 432), aspartate (*m*/*z* 302, 390 and 418), glycine (*m*/*z* 218 and 246), alanine (*m*/*z* 232 and 260), serine (*m*/*z* 362 and 390), methionine (*m*/*z* 218 and 320), cysteine (*m*/*z* 406), phenylalanine (*m*/*z* 336), valine (*m*/*z* 260), leucine (*m*/*z* 274), isoleucine (*m*/*z* 274), tyrosine (*m*/*z* 302). Data were normalized to the total protein content of each sample with a Pierce™ BCA Protein Assay Kit (Thermo Scientific™; catalog no. 23227). For metabolic flux analysis, mass range of 100–600 was analyzed, recorded at 1,562 mass units/second. The 'M-57′ fragment was were detected as TBDMS derivatives. IsoCor software was used to adjust for natural abundance as previously performed [21].

LC-MS analysis

For metabolite extraction, 20 individual tissues (fat body, ovary or guts) or ten whole bodies were pooled to form one sample, respectively. The samples were mixed with 1 mL of acetonitrile/methanol/H_2O (*v*/*v*/*v* = 2:2:1) containing 100 μM internal standards (Methionine sulfone) to precipitate the proteins. The frozen tissues or whole bodies were ground using a homogenizer and stored at −20 °C for 2 h. After centrifugation at 4 °C and 14,000 × g for 15 min, the supernatant was transferred to a new Eppendorf tube and dried in a vacuum concentrator at 37 °C. The dry pellets were reconstituted into 50 μL or 100 μL of acetonitrile/methanol/H_2O (*v*/*v*/*v* = 2:2:1) and sonicated for 10 min. Samples were analyzed using a UPLC-ESI-TSQ-MS/MS system separated through a Dionex UltiMate 3000 UPLC system and TSQ Quantis Mass (ThermoFisher, USA). Mobile phase A was water with 10 mM ammonium acetate, pH 9.0, and mobile phase B was acetonitrile with 10 mM ammonium acetate, pH 9.0. For metabolite analysis, we used a hydrophilic interaction liquid chromatography (HILIC) method, with an Infinity Lab Poroshell 120 HILIC column (100 × 2.1 mm internal diameter, 2.7 μm; Agilent) for compound separation at room temperature. The flow rate was set at 0.3 mL/min and the injection volume was 5.0 or 10 μL. The samples were eluted with the following linear gradient: 95–50% B, 0–10 min; 50–95% B, 10–13 min; 95% B, 13–16 min. The ion transfer tube and vaporizer temperatures were set at 350 °C and 325 °C, respectively. The sheath gas (N2) flow rate was 50 psi, auxiliary gas flow rate was 10 psi, and the ion spray voltage was set at 2.5 kV and negative electrospray ionization (ESI−). Selected reaction monitoring (SRM) was used and the following metabolites were detected: AMP (*m*/*z* 346 to 134), ADP (*m*/*z* 426 to 328), R5P (*m*/*z* 229 to 97), GSH (*m*/*z* 306 to 143), DF6P (*m*/*z* 259 to 97), S7P (*m*/*z* 289 to 199), ATP (*m*/*z* 506 to 408), NADPH (*m*/*z* 744 to 426), G6P (*m*/*z* 259 to 199), E4P (*m*/*z* 199 to 97), DHAP (*m*/*z* 169 to 97), NADP+ (*m*/*z* 742 to 408), GSSG (*m*/*z* 611 to 306), F16BP (*m*/*z* 339 to 97). Data were normalized to the total protein content of each sample with a Pierce™ BCA Protein Assay Kit (Thermo Scientific™; catalog no. 23227).

Furthermore, for the detection of SAM, SAH and acetyl-CoA, LC separations were performed on an Agilent Infinity Lab Poroshell 120 HILIC-Z. The mobile phase consisted of 10 mM ammonium acetate in water (solvent A) and 10 mM ammonium acetate in acetonitrile (solvent B). The total run time was at 16 min. The samples were eluted with the following linear gradient: 95–50% B, 0–5 min; 50–20% B, 5–8 min; 20–5% B, 8–10 min; 5–95% B, 10–13 min; 95% B, 13–16 min. The polarity is positive ion. Selected reaction monitoring (SRM) was used and the following metabolites were detected: SAM (*m*/*z* 400 to 250), SAH (*m*/*z* 386 to 136.5), and acetyl-CoA (*m*/*z* 810 to 303). For metabolic flux analysis, citrate (*m*/*z* 191 to 196) and acetyl-CoA (*m*/*z* 809 to 811) was analyzed with SRM mode. IsoCor software was used to adjust for natural abundance as previously reported [21].

RNA sequencing analysis and quantitative RT-PCR analysis

For RNA sequencing analysis, 50 female flies were pooled for each experimental group, total RNA was extracted using TRIzol reagent (Thermo Scientific™; catalog no. 15596026) and the integrity was assessed using a Nano 6000 Assay Kit of the Bioanalyzer 2100 system (Agilent Technologies, CA, USA). mRNA was purified from the samples using poly-T oligo-attached magnetic beads. For library preparation, briefly, cDNA was synthesized using random hexamer primer, M−MuLV Reverse Transcriptase, and DNA

Polymerase I. Then the cDNA fragments of preferentially 370 ~ 420 bp in length were purified with AMPure XP system (Beckman Coulter, Beverly, USA) and PCR was performed with Phusion High-Fidelity DNA polymerase, Universal PCR primers and Index (X) Primer. The library quality was verified using the Agilent Bioanalyzer 2100 system. The library samples were forwarded to a cBot Cluster Generation System for RNA sequencing using an Illumina Novaseg platform and 150 bp paired-end reads were generated. The paired-end 150-base pair sequence data were analyzed as follows: A quality check of the raw reads was performed by FastQC (v0.12.1) and MultiQC (v1.14). The raw reads were then filtered to remove the adaptors and low-quality bases using Trim Galore (v0.6.10). Filtered reads were aligned to the Drosophila genome (BDGP6.46) using Hisat2 (v2.2.1). The read counts were calculated using StringTie (v2.2.1). Differentially expressed genes were identified using edgeR (v4.0.6).

For quantitative RT-PCR analysis, total RNA was extracted from the ten adult female flies using TRIzol reagent. The cDNA was synthesized from 1000 ng of deoxyribonuclease-treated total RNA using Oligo$(dT)_{18}$ primer, M–MLV RT Buffer (Invitrogen; catalog no. 2757096), and M–MLV Reverse Transcriptase (Invitrogen; catalog no. 2985244). Quantitative RT-PCR was performed using Taq Pro Universal SYBR qPCR Master Mix (Beyotime; catalog no. D7260) and analyzed on a Bio-Rad CFX96™ Real-Time System (Hercules, CA, USA). Primer sequences are listed in Table 1 [18,19,22].

Histone extraction and Western blot analysis

Approximately 40 female flies or 20 ovaries were homogenized with 600 μL or 100 μL RIPA lysis buffer (Thermo Scientific™; catalog no. 89900) supplemented with deacetylase inhibitor (Beyotime; catalog no. P1113), protease and phosphatase inhibitor (Thermo Scientific™; catalog no. 78440). The supernatant was collected after centrifugation, and the protein amount was determined with a a Pierce™ BCA Protein Assay Kit (Thermo Scientific™; catalog no. 23227). The samples were mixed with 5 × SDS-polyacrylamide gel electrophoresis (SDS-PAGE) sample buffer (Beyotime; catalog no. P0015). and about 40 μg proteins were subjected to standard SDS-PAGE. Gels were transferred to the polyvinylidene difluoride membrane and blocked by Tris-buffered saline containing 5% of bovine serum albumin (BSA, Beyotime, catalog no. ST023). The blots were incubated overnight at 4 °C with anti-H3K27me3 (1:1000, Abcam, catalog no. ab6002), anti-H3K27ac (1:1000, Abcam, catalog no. ab177178), anti-H3K9ac (1:1000, Abcam, catalog no. ab32129), anti-H3.3 (1:1000, Abcam, catalog no. ab176840), anti-H3K4me3 (1:1000, Abcam, catalog no. ab8580), anti-H3K9me3 (1:1000, Abcam, catalog no. ab8898), anti-H3K36me3 (1:1000, Abcam, catalog no. ab9050), or anti-H3 (1:1000, Abcam, catalog no. ab1791) antibodies in Tris-buffered saline, 0.05% Tween 20 (TBS-T), containing 3% of BSA. After five washes for 5 min with TBS-T, blots were incubated for 1 h at room temperature with horseradish peroxidase-conjugated anti-rabbit secondary antibody (LICORbio™; catalog no. 926–80010) diluted 1:5000 or 1:1000 in TBS-T containing 3% of BSA. Blots were washed again and bands were visualized using enhanced chemiluminescent reagent (BeyoECL Star; catalog no. P0018). Densitometry quantification was achieved using ImageJ software (version 1.53, NIH, Bethesda, MD, USA).

Statistical analysis

Statistical analysis was performed using GraphPad Prism 10 (GraphPad Software, San Diego, CA, USA). A log-rank test was used to compare statistical significance for the survival curve. An unpaired and two-sided Student's *t-test* was used to compare samples. One-way analysis of variance (ANOVA) with Tukey's multiple comparisons test was used to compare groups. One-way ANOVA with Tukey's multiple comparisons test was used to compare against a control sample. Bar graphs are drawn as the means and standard error of the mean (S.E.M). *P* values are depicted on the figures; $^{*}P < 0.05$; $^{**}P < 0.01$; $^{***}P < 0.001$; $^{****}P < 0.0001$.

Results

Administration of EGCG increases the resistance of male parents and offspring to infections in mice

To test whether parental administration of EGCG enhances immunity in offspring, 5-week-old mice were intragastrically (i.g.) daily fed with EGCG (300 mg/kg body weight) for 6 weeks. Only male mice were employed to avoid the influence of the estrous cycle or the uterine environment of the animals. After six weeks of administration, both control mice (intragastric PBS, F0) and EGCG-exposed mice (intragastric EGCG, F0) were subjected to a systemic intraperitoneal (i.p.) injection of *Escherichia coli*. The other male mice (control and EGCG-exposed mice) without infection were bred with healthy naive females to generate the first offspring of these mice, termed F1 control and F1 EGCG-exposed lineages, respectively. Following six to eight weeks of normal diet administration, these independent mice were subsequently subjected to the same *E. coli* systemic infection at the same dosage (Fig. 1A). Weight gain was monitored in both F0 and F1 generations (Fig. 1, B and C), while food intake was determined only in the F0 generation (Fig. 1D). EGCG-exposed mice failed to exhibit a significant weight difference compared to the control mice. However, the offspring of EGCG-exposed mice showed a greater weight gain than that of the offspring of control mice. In addition, although the food intake was altered in the first two weeks, it remained stable during the following four weeks.

To evaluate the capacity of host defense, we compared the bacterial burden in the kidney, lung, liver, and spleen of the mice at 12 h and 36 h post infection. F0 EGCG-exposed mice showed a reduction of bacterial burden in the kidney, lung, and spleen (Fig. 1E). Furthermore, an increased recruitment of cMOP cells was also observed in F0 mice at 36 h post infection (Fig. 1F). Similarly, F1 EGCG-exposed male mice also exhibited a reduction of bacterial burden in the lung and liver (Fig. 1G). However, female offspring failed to improve enhance this resistance (Fig. 1H). The rapid immune response contributes to enhanced bacterial resistance, as reflected by the production of pro-inflammatory factors [23]. F0 and F1 EGCG-exposed mice showed higher levels of TNF-α levels (Fig. 1I), and the serum TNF-α still kept to be elevated in F1 mice at 4 h post infection (Fig. 1J).

The rapid assembly of the immune system requires a large amount of energy [24]. This was usually accompanied by the consumption of glucose and triglycerides [25]. A reduction of serum glucose and triglycerides was detected in EGCG-exposed mice (Fig. 1K). However, only F1 EGCG-exposed male mice showed lower levels of triglycerides rather than females, suggesting a gender-specific effect (Fig. 1, L and M).

Parental early-life EGCG exposure induces host defense against pathogen infection across generations in Drosophila melanogaster

Next, we investigated whether the transgenerational effect of EGCG on host defense could be conserved in invertebrates. The fruit fly *Drosophila melanogaster* is a well-recognized model for studying genetic diseases and the response of pathogens due to its high relevance to mammalian biology in terms of key signal transduction pathways and transcriptional regulators that control

Table 1
Primer sequences used in this study.

Gene name (FlyBase ID)	Forward	Reverse
rp49 (FBgn0002626)	CGTTTACTGCGGCGAGAT	CCGTTGGGGTTGGTGAG
relish (FBgn0014018)	CTTAATGGAGTGCCAACCGT	TGCCATGTGGAGTGCATTAT
dpt (FBgn0004240)	GCTGCGCAATCGCTTCTACT	TGGTGGAGTGGGCTTCATG
atta (FBgn0012042)	CCCGGAGTGAAGGATG	GTTGCTGTGCGTCAAG
drs (FBgn0283461)	CGTGAGAACCTTTTCCAATATGATG	TCCCAGGACCACCAGCAT
ceca1 (FBgn0000276)	GAACTTCTACAACATCTTCGT	TCCCAGTCCCTGGATT
hexa (FBgn0001186)	ATATCGGGCATGTATATGGG	CAATTTCGCTCACATACTTGG
pgi (FBgn0003074)	ACTGTCAATCTGTCTGTCCA	GATAACAGGAGCATTCTTCTCG
pfk (FBgn0003071)	AGCTCACATTTCCAAACATCG	TTTGATCACCAGAATCACTGC
gapdh1 (FBgn0001091)	TTGTGGATCTTACCGTCCGC	CTCGAACACAGACGAATGGG
eno (FBgn0000579)	CAACATCCAGTCCAACAAGG	GTTCTTGAAGTCCAGATCGT
pglym78 (FBgn0014869)	TCCCCATCCAGAAGACTTGG	TGACGATGTTCTCGTAGTACGG
pyk (FBgn0267385)	GTTTACGGTGCGTCTTAATGGA	CGTGCTTCTCGTGAGCCTC
pdh1 (FBgn0028325)	GTGTCCACGGATGGACCTAC	CCATGTTGTAAGCCTCGAACAC
ldh (FBgn0001258)	ACGGCTCCAACTTTCTGAAG	GCAAAATGGTATCGGGACTG
p300/cbp (FBgn0261617)	TGCGGCAGGAAGTACACATT	TCTATTTGAGGCGACACCGT
acly (FBgn0020236)	GTGGAAAGCTGGGACTAATTGG	GCGAGTAGATGCACACGTACA
dtor (FBgn0003733)	GAATTGTGGGCAGATGACCT	CCTGCCTGTTGCACTGATTA
ampkα (FBgn0023169)	GGCCATCGCTTACCATCTGA	ATCGATGATTGGGGAACGGG
myc (FBgn0262656)	TGTCCTCGATGTGCTCAACC	GTCACTATCAGAGCCGGTCG
atf4 (FBgn0000370)	AGGCCATAGTACCCGCAAAC	CCGCCTGTTTGTAAGCATCG
foxo (FBgn0038197)	AACAACAGCAGCATCAGCAG	CTGAACCCGAGCATTCAGAT
sima (FBgn026641)	AACTATCGCGAGGAGTCGAA	CGTTAGCAGGGGCATATCAT

development, metabolism, and immunity [26]. To test the transgenerational effects of EGCG-induced host defense, we first fed adult male *Drosophila* with EGCG-rich food (2 mM and 10 mM) for six days, subsequently mating with naive females from a normal diet to generate the first generation (F1, Fig. S1A). After being fed with four to seven days of a normal diet, the F1 offspring were then subjected to the systemic needle pricking infection of *Pseudomonas aeruginosa* strain PA14. However, the male offspring from EGCG-exposed males failed to show an increasing survival rate after infection (Fig. S1B). Consequently, survival rates of 10 mM EGCG-exposed females and their female offspring was determined with the same intervention routes (Fig. 2A). Another gram-positive bacterium, *Staphylococcus aureus*, was also used for infection to confirm hypothesis. In contrast, a significant increase in survival rates after *P. aeruginosa* infection was observed in the EGCG-exposed females and their female offspring, the transgenerational effect was detected in the F2 generation (Fig. 2C), while only the F0 generation showed an increasing survival rate after *S. aureus* infection (Fig. 2B). Moreover, we also tested the bacterial burden of whole body 6 h after *P. aeruginosa* infection. Only the F0 generation showed a reduction of bacterial burden, while F1 did not (Fig. 2D). The administration of EGCG induced a gender-specific and heterogeneous host defense against different types of pathogens across generations in *D. melanogaster*.

To determine whether extension of EGCG exposure could enhance its transgenerational effect, embryos from adult females mating with males were laid on the surface of 10 mM EGCG-rich food (Fig. 2A). The females after eclosion were continuously subjected to EGCG exposure until infection or mating on normal yeast-based diet to generate multiple generations of offspring (EGCG-F1 to –F3 flies). With this design, EGCG-F1 to –F3 flies and controls were all maintained on a normal yeast-based diet food from their embryo stage, thus any observed metabolic and survival differences among them were likely attributed to ancestral exposure to EGCG and its transgenerational effect on offspring. Obviously, the survival assay showed an increasing survival rate after *P. aeruginosa* and *S. aureus* infection in females from embryos exposed to EGCG and their F2 female offspring (Fig. 2, E and F). The bacterial burden 6 h after *P. aeruginosa* infection was also significantly decreased from F0 to F2 generation (Fig. 2G). Consistent with previous results, the males and their offspring did not show significance after *P. aeruginosa* infection (Fig. S1, C and D), confirming the gender-specific effect of EGCG. We next quantified fecundity (egg-laying) and developmental states (pupal number) to EGCG exposure. Flies exposed to EGCG for six days showed no differences in the number of eggs (Fig. S2A). Pupal numbers exhibited an initial increase followed by a decrease during EGCG exposure (Fig. S2B). However, this phenotype was reversed in the F1 generation with pupal counts returning to baseline levels (Fig. S2C).

The secretion of antimicrobial peptides (AMPs) is the predominant pathway of humoral immunity of *Drosophila* and rapidly induced following microbial infection [27]. We next analyzed the expression of AMP-related genes at 3 h and 6 h post *P. aeruginosa* infection in F0 and F1 generations (Fig. 2, H and I). The expression of *diptericin* (*dpt*) and *attacin A* (*atta*) genes was higher 6 h after infection in the F0 generation. While the expression of *cecropin A1* (*ceca1*) and *drosomycin* (*drs*) genes was higher 3 h and 6 h after infection in the F1 generation. The rapidly induced AMP-related gene expression could contribute to the increasing survival rates after bacterial infection in F0 and F1 generations. Building upon these findings, we aimed to elucidate the potential transgenerational mechanisms of immune priming in flies whose embryos were further exposed to EGCG. To investigate how long the resistance to infections can be remained in EGCG-exposed flies. EGCG-exposed flies (6 days old) were switched to a yeast-based food for 6 and 24 days (Fig. S3A). Interestingly, flies with previous EGCG exposure still showed an increasing survival rates at the 6th day, while disappearing at the 24th day (Fig. S3, B and C). In contrast, 30-days old F1 flies exhibited a robust protection against *P. aeruginosa* (Fig. S3, A, C, and D), suggesting that EGCG-triggered host defense may have a memory effect both in F0 and F1 generations.

EGCG activates glycolysis to support anabolism

We hypothesized that the proliferation of immune cells correlates with the increasing AMPs-related gene expression and warranting for cells to switch to aerobic glycolysis rather than oxidative phosphorylation, which is also called as "Warburg effect" [28]. The aerobic glycolysis contributes to the biosynthesis of many substrates including nucleotides, lipids, and proteins (Fig. 3A). Based on RNA sequencing analysis, we found a large number of dif-

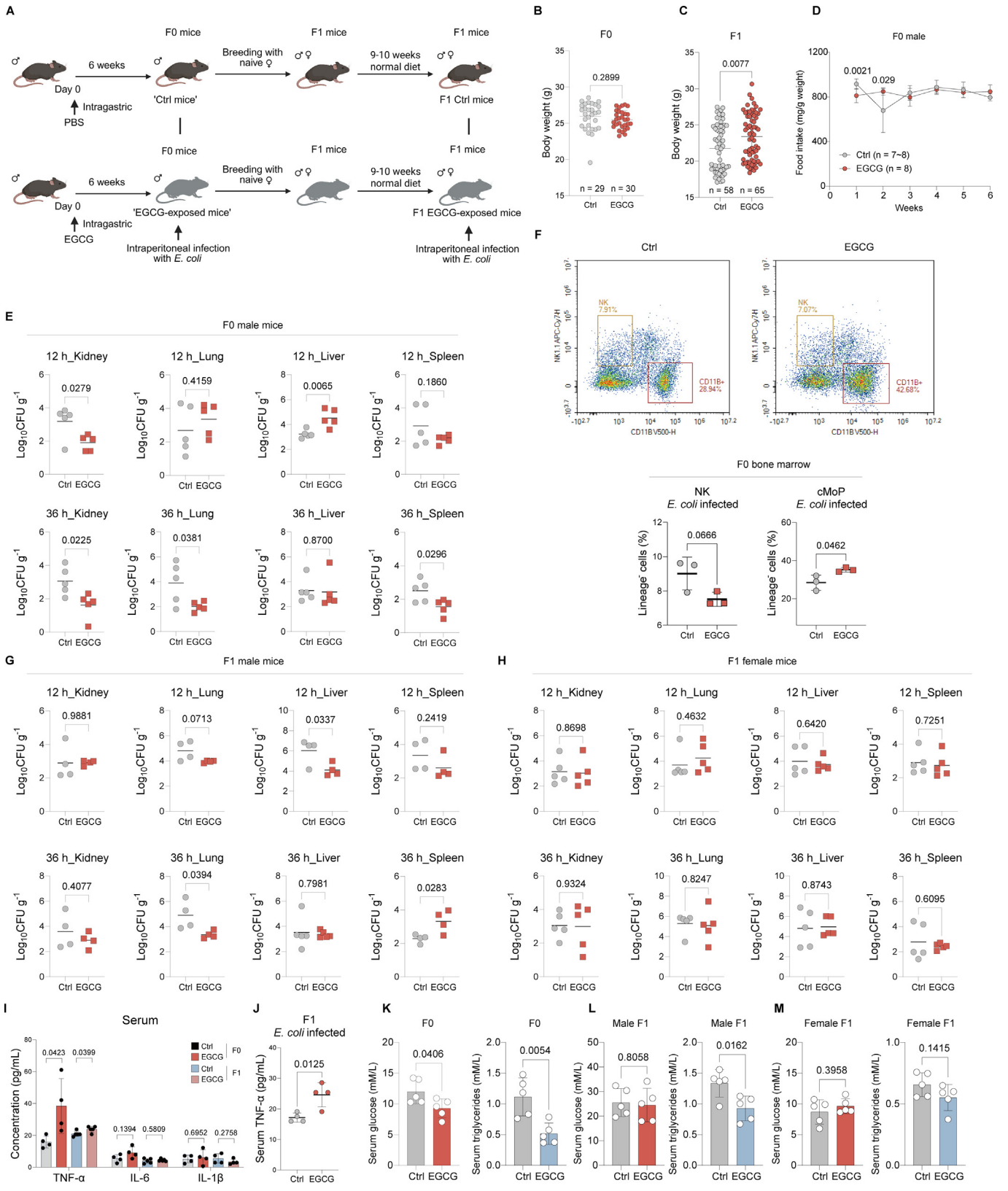

Fig. 1. Administration of EGCG increases the resistance of male parents and offspring to infections in mice. (A) Scheme of the experimental procedures followed in mice. Created with BioRender.com. (B) Body weight gain after 6-weeks administration in F0 mice. Sample sizes (n) are shown in the figure. (C) Body weight gain after 9- or 10- weeks of normal diet administration in F1 mice. Sample sizes (n) are shown in the figure. (D) Food intake changes during six-weeks EGCG administration in paternal mice. n = 7 ~ 8 biological replicates. (E) Bacterial burden assessed from kidney, lung, liver and spleen 12 and 36 h intra-peritonelly (i.p.) infection with *E. coli* in F0 male mice. n = 4 ~ 5 mice per group. (F) Flow cytometry analysis and percentages of NK and cMoPs cells present in the bone marrow of paternal mice 36 h after i.p. *E. coli* infection. NK, natural killer cells; cMoPs, common monocyte progenitors. n = 3 mice per group. (G and H) Bacterial burden assessed from kidney, lung, liver and spleen 12 and 36 h intra-peritonelly (i.p.) infection with *E. coli* in F1 male (G) and female (e) mice. n = 4 ~ 5 mice per group. (I) Circulating TNF-α, IL-6, and IL-1β concentrations in the blood of F0 and F1 mice. n = 4 ~ 5 mice per group. (J) Circulating TNF-α concentrations 12 h after i.p. infection with *E. coli* in the blood of F1 mice. n = 4 ~ 5 mice per group. (K-M), Circulating glucose and triglyceride in the blood of F0 (K), male F1 (L) and female F1 (M) mice. n = 5 mice per group. Statistical significance was calculated by two-tailed Student's t-tests. Error bars represent S.E.M. *P* values are depicted on the figures; $^{*}P < 0.05$; $^{**}P < 0.01$; $^{***}P < 0.001$; $^{****}P < 0.0001$.

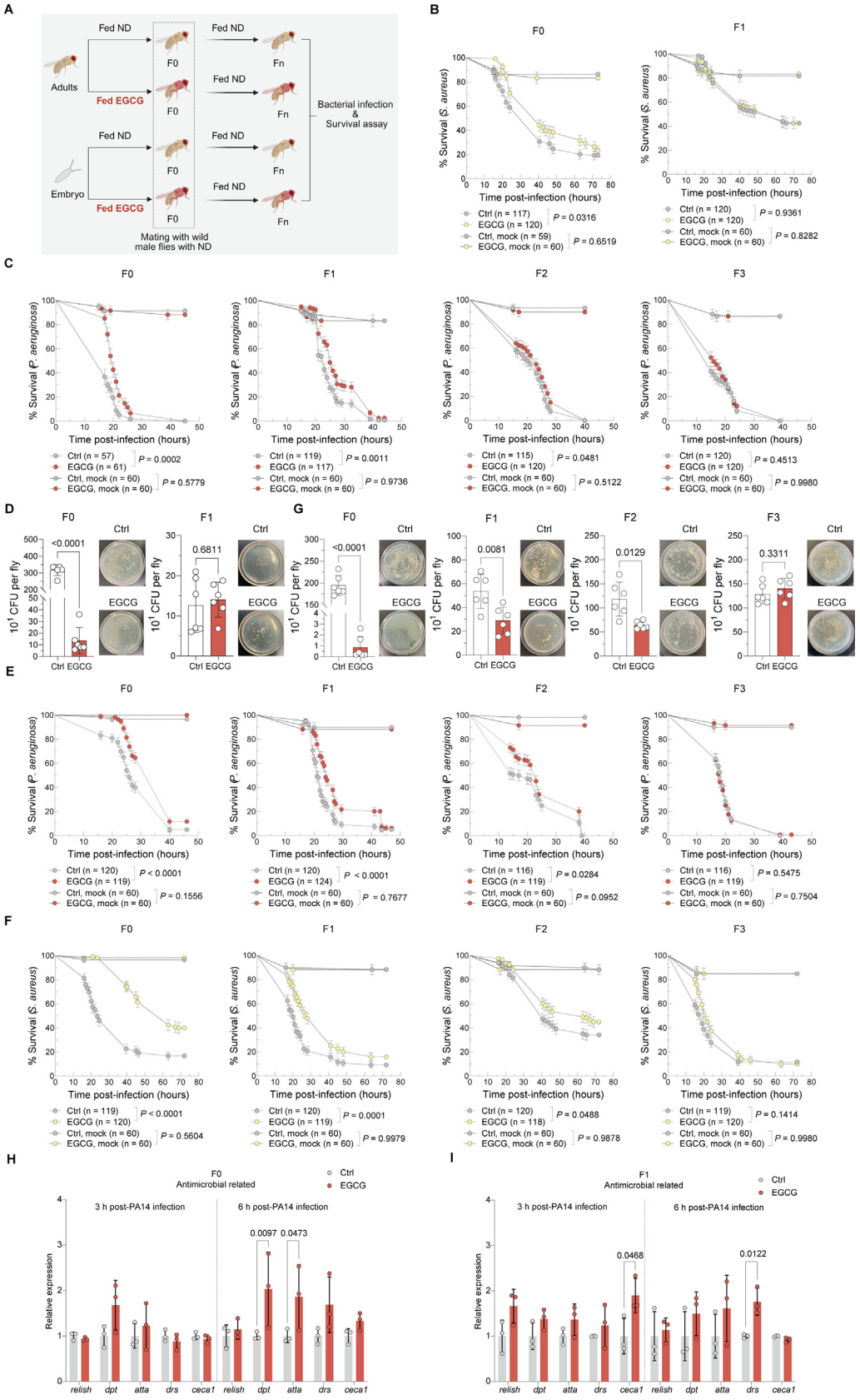

Fig. 2. Parental early-life EGCG exposure induces host defense against pathogen infection across generations in *Drosophila melanogaster*. (A) Scheme of the experimental procedures followed in flies. Created with BioRender.com. (B and C) Survivorship on female adult flies from 6 days with or without EGCG diet administration and its female offspring following *S. aureus* (B) and *P. aeruginosa* (C) infection. Sample sizes (n) are shown in the figure. (D) Bacterial load assessed from individual flies 6 h after *P. aeruginosa* infection in F0 and F1 flies from adult females with or without EGCG diet administration. n = 6 biological replicates per group. (E) Survivorship on female adult flies from embryos with or without EGCG diet administration and its female offspring following *P. aeruginosa* (E) and *S. aureus* (F) infection. Sample sizes (n) are shown in the figure. (G) Bacterial load assessed from individual flies 6 h after *P. aeruginosa* infection in F0, F1, F2, and F3 flies from embryos with or without EGCG diet administration. n = 6 biological replicates per group. (H and I) Relative mRNA levels of antimicrobial-related genes 3 or 6 h after *P. aeruginosa* infection in F0 (H) and F1 (I) flies. n = 3 biological replicates per group. For survivorship, mock injury groups are displayed and statistical significance was calculated by the log-rank test. For statistical analyses between two samples, two-tailed Student's t-tests were used. Error bars represent S.E.M. *P* values are depicted on the figures; $^{*}P < 0.05$; $^{**}P < 0.01$; $^{***}P < 0.001$; $^{****}P < 0.0001$.

ferentially expressed genes (DEGs) in F0 and F1 whole flies (Fig. S4, A and B). In particular, we selected top 20 metabolism-related pathways by KEGG enrichment analysis in flies. Alterations in amino acid metabolism and biosynthesis, CoA synthesis, as well as glycolysis/gluconeogenesis pathways were observed in both F0 and F1 flies (Fig. S4, C and D). Further quantitative PCR analysis in F0 and F1 flies showed a remarkable change in glycolysis pathway (Fig. 3, B and C). Notably, the gene expression of *phosphofructokinase* (*pfk*), a key rate-limiting enzyme in glycolysis, was significantly upregulated in both F0 and F1 flies. In contrast, the expression of *pyruvate kinase* (*pyk*), the terminal rate-limiting enzyme in the same pathway, was markedly downregulated in both generations (Fig. 3, B and C). This opposing pattern reflects a metabolic shift to balance energy production with biosynthetic and redox demands under altered physiological conditions. The concurrent increase in body weight and reduction in glucose and triglyceride levels in F0 and F1 flies suggest that a pronounced metabolic reprogramming takes place (Fig. S2, D and E; Fig. 3, D–G). In addition, body weight remained unchanged in the F2 and F3 generations (Fig. S2, F and G).

To further investigate the underlying metabolic changes, targeted metabolite profiling was performed using gas or ultra performance liquid chromatography coupled with mass spectrometry (GC–MS or UPLC-MS/MS). Firstly, metabolite profiles of the whole body in F0 females from embryos exposed to an EGCG-rich or a normal yeast-based diet and F1 females was acquired. Although EGCG-exposed females were not so clearly separated from control females (Fig. 3H), differences between them in both F0 and F1 flies could still be observed to encompass pathways such as glycolysis-TCA cycle-, phosphopentose-, redox-, energy-, nucleotide-, and amino acids-related metabolites (Fig. 3I). As expected, glycolysis-related metabolites such as phosphoenopyruvate and lactate were increased in EGCG-exposed F0 and F1 flies. Likewise, an accumulation of tricarboxylic acid (TCA) cycle-related metabolites was evident, accompanied by increased adenosine monophosphate levels, suggesting a reduction in cellular energy status. Moreover, the fold-increase levels of amino acids, such as serine, indicated a metabolic shift in EGCG-exposed flies toward biosynthetic processes rather than energy production (Fig. 3I). The fat body in *Drosophila,* as the central metabolic organ, plays a crucial role in nutrient sensing, energy storage, and metabolic homeostasis. We next generated the metabolite profiles of the fat body in F0 and F1 flies as before (Fig. 3, J and K). The glycolysis-related metabolites showed a much more significant increase in EGCG-exposed flies. In addition, the substrate of nucleotides, ribose 5-phosphate, showed accumulation in both F0 and F1 generations. Interestingly, an increase in the amino acid levels was not observed in the fat body of F0 flies following EGCG exposure (Fig. 3, J and K), which may be attributed to enhanced utilization for protein synthesis.

To investigate how EGCG supports anabolism, we carried out an isotope tracing (U-$^{13}C_6$-glucose) approach to quantify metabolic flux in the fat body and whole body of flies (Fig. 3L). In order to achieve glucose metabolic homeostasis, two different time points (24 h and 48 h) were chosen to collect samples [20]. In F0 flies, glucose-derived labelling of m + 3 lactate showed a decreased level in the fat body after 24 h, while increased in whole body after 48 h, indicating a time-dependent and tissue-specific rewiring of glucose metabolism (Fig. 3, M and N). Interestingly, we found labelling of m + 3 lactate remained elevated with a higher fold-change in both fat body and whole body (Fig. 3, M and N), implying a significantly increased glycolytic activity. In contrast, the labelling of m + 2 succinate and m + 2 fumarate remained largely unchanged in fat body or whole body of F0 and F1 flies (Fig. 3, M and N), confirming that EGCG promotes glycolytic activity rather than TCA cycle activity. Additionally, the flux of alanine (m + 3) derived from pyruvate and serine (m + 3) derived from 3PG were observed to be increased (Fig. 3, M and N) in F0 and F1 whole body. Notably, serine serves as a substrate for one-carbon units which are directly to the synthesis of nucleotides. Taken together, our data indicates that EGCG exposure promoted the glycolytic activity to increase anabolism including amino acid biosynthesis, one-carbon units, lipids and nucleotides in F0 and F1 flies. Such metabolic reprogramming is required to sustain the macromolecule biosynthesis required for the rapid proliferation of immune cells.

H3K27ac correlates with the immune priming in offspring

Changes in gene expression are known to be transmitted from one generation to the next through inheritance of epigenetic modifications [29]. Given the important roles of histone modifications in epigenetic regulation, we sought to investigate which types of histone modifications were altered in the EGCG-induced intergenerational inheritance of immune priming. Thus, we first monitored levels of seven types of histone modifications that are widely reported in F1 *Drosophila,* including H3.3, H3K9ac, H3K27ac, H3K27me3, H3K4me3, H3K9me3, and H3K36me3 (Fig. 4A). The levels of H3K27ac were significantly increased in the whole body of F1 flies (Fig. 4A). Further assays revealed that the increasing H3K27ac levels were only transmitted from the F0 to the F1 generation (Fig. 4B).

Several studies have demonstrated that H3K27ac modification is of great significance in the "trained immunity" and can induce gene expression involved in glycolysis [30]. To determine whether H3K27ac is a key epigenetic regulator of transgenerational EGCG-driven host defense, we reduced H3K27ac levels by inhibiting the lysine acetyltransferase (KAT) using curcumin, a natural target of p300/CBP (KAT) inhibitor (Fig. 4, C and D) [31]. Interestingly, treatment with curcumin (10 and 50 mM for 4 days) eliminated increased survival rates of F1 EGCG-exposed females after *P. aeruginosa* infection but not in F0 females. This indicates that increasing H3K27ac is highly associated with host defense in the offspring of EGCG-exposed flies.

Nuclear acetyl-CoA is a core metabolite and the sole donor of H3K27ac modification. We further investigated the availability of acetyl-CoA in F0 and F1 flies. The acetyl-CoA was accumulated in either the whole body or the fat body of F0 and F1 generations (Fig. 4, E-H). Acetyl-CoA synthetase 2 (ACSS2) and ATP-citrate lyase (ACLY) are two key acetyl-CoA synthetases that generate nuclear acetyl-CoA from acetate and citrate, respectively [5]. No changes in gene expression of *p300/cbp* and *acly* was observed in flies (Fig. 4J). Given the reduction of glucose level in F1 females (Fig. 4, D and E), we hypothesized that citrate derived from glucose was the precursor of acetyl-CoA. Through isotope tracing with U-$^{13}C_6$-glucose in the whole-body flies, as previously performed (Fig. 4I), we found that while citrate (m + 2) flux remained unchanged, acetyl-CoA (m + 2) flux was markedly elevated in F1 females, consistent with enhanced cytosolic acetyl-CoA generation from glucose, rather than citrate-derived acetyl-CoA shuttling (Fig. 4, K and L).

The mTOR- and HIF-1α-mediated aerobic glycolysis has been recognized as the metabolic basis for the "trained immunity" [30] To investigate whether the EGCG-induced host defense in F1 generation is also linked with mTOR activation, we examined the survival rate of F1 EGCG-exposed females under three days of rapamycin or metformin (mTOR inhibitors) treatment after *P. aeruginosa* infection. Inhibition of mTOR did not eliminate this effect (Fig. 4, M and N). In addition, the circulating lactate in hemolymph and global level of *sima* (the *Drosophila* HIF-1α ortholog) in the whole body did not exhibit an increase in F1 generation at 3 h post infection (Fig. 4, O and P). These findings suggest that EGCG-induced host defense did not rely on the mTOR activation in F1 flies.

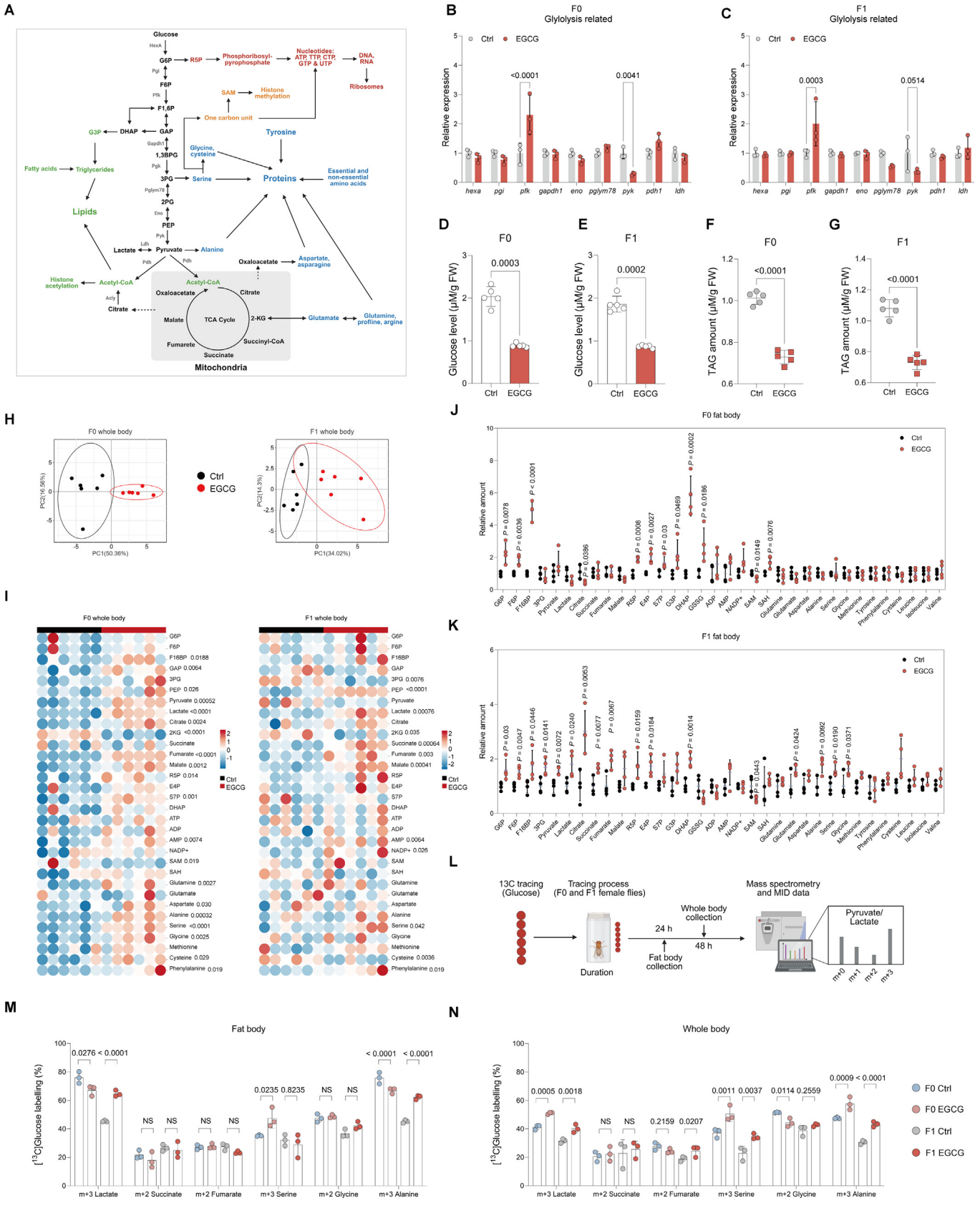
A
Glucose
G6P
R5P
Phosphoribosyl-pyrophosphate
Nucleotides: ATP, TTP, CTP, GTP & UTP
DNA, RNA
Ribosomes
F6P
F1,6P
SAM
Histone methylation
One carbon unit
Tyrosine
G3P
DHAP
GAP
1,3BPG
Glycine, cysteine
Fatty acids
Triglycerides
3PG
Serine
Proteins
Essential and non-essential amino acids
Lipids
2PG
PEP
Lactate
Pyruvate
Alanine
Oxaloacetate
Aspartate, asparagine
Histone acetylation
Acetyl-CoA
Citrate
Malate
TCA Cycle
2-KG
Glutamate
Glutamine, proline, argine
Fumarete
Succinyl-CoA
Succinate
Mitochondria
B
F0
Glylolysis related
Ctrl
EGCG
Relative expression
<0.0001
0.0041
hexa
pgi
pfk
gapdh1
eno
pglym78
pyk
pdh1
ldh
C
F1
Glylolysis related
0.0003
0.0514
D
F0
0.0003
Glucose level (μM/g FW)
E
F1
0.0002
F
F0
<0.0001
TAG amount (μM/g FW)
G
F1
<0.0001
H
F0 whole body
F1 whole body
PC1(50.36%)
PC2(16.56%)
PC1(34.02%)
PC2(14.3%)
I
F0 whole body
F1 whole body
J
F0 fat body
Relative amount
K
F1 fat body
L
13C tracing (Glucose)
Tracing process (F0 and F1 female flies)
Mass spectrometry and MID data
Whole body collection
24 h
48 h
Fat body collection
Duration
Pyruvate/ Lactate
m+0
m+1
m+2
m+3
M
Fat body
[13C]Glucose labelling (%)
0.0276
< 0.0001
0.0235
0.8235
< 0.0001
m+3 Lactate
m+2 Succinate
m+2 Fumarate
m+3 Serine
m+2 Glycine
m+3 Alanine
N
Whole body
0.0005
0.0018
0.0011
0.0037
0.0114
0.2559
0.0009
F0 Ctrl
F0 EGCG
F1 Ctrl
F1 EGCG

EGCG reduces intestinal amino acids to trigger the integrated stress response

Our previous investigation showed that flavonoids such as EGCG with pyrogallol moiety in ring B could react with amino acids (AAs) and form ammoniation products at 37 °C [32,33]. This implies that EGCG may reduce the levels of amino acids by nonenzymatic degradation. *Drosophila* larvae obtain nutrients and yeast from the medium to support their development, and the intestinal tract is the primary site of exposure to EGCG. To investigate the effect of host defense in F0 EGCG-exposed females, metabolite profiling was performed in the intestine of F0 flies. As expected, EGCG significantly reduced the amount of five essential amino acids (EAAs) including valine, leucine, isoleucine, phenylalanine, and methionine (Fig. 5A). Tyrosine, as a non-essential amino acid (NEAA), was also decreased in the intestine (Fig. 5A). Glycolysis- and TCA cycle-related metabolites remained unchanged (Fig. 5B). Notably, the total contents of phenylalanine and leucine in flies were increased in flies, while valine, isoleucine, and tyrosine were remained unchanged (Fig. 3I and Fig. 5C). The result indicates that EGCG-induced intestinal AAs deficiency may be sensed by fly body and perhaps alter intake or excretion of various AAs. It is also possible that free AAs are increased through enhanced protein degradation such as autophagy pathway [34].

AAs deficiency can activate nutrient-sensing mechanism in animals, including insulin/insulin-like growth factor 1 signaling (IIS), mechanistic target of rapamycin complex 1 (mTORC1), and general control nonderepressible 2 (GCN2)–activating transcription factor 4 (ATF4) [35]. We found that GO terms related to substance transport and ion transmembrane transport pathways were significantly remodeled under intestinal AAs deficiency in F0 flies (Fig. 5D). This result was accompanied by the upregulation of protein digestion and absorption and downregulation of basal transcription factors by GSEA enrichment analysis (Fig. 5, E and F). We also identified 20 upregulated genes and 2 downregulated genes encoding proteins involved with amino acid restriction (Fig. 5G). While increased *atf3* (a target transcription factor of *atf4*) and *atf4* were observed in the EGCG group. Further quantitative real-time PCR results demonstrated that *atf4* was significantly increased in F0 EGCG-exposed whole flies (Fig. 5H). ATF4 is the fundamental effector that activates the integrated stress response (ISR) during various stress conditions, including endoplasmic reticulum (ER) stress and viral infection [35]. The activation of ATF4 has been reported to induce "Warburg metabolism", thereby driving over proliferation in *Drosophila* [36], which is consistent with our previous results. In addition, the restriction of some AAs, such as methionine and tyrosine, can extend lifespan, we also observed this phenomenon in the F0 generation, while the F1 generation did not (Fig. 5, I and J). As reported previously [37], a decline of dietary tyrosine induced the reduction of ovary size, which was also observed in F0 EGCG-exposed flies (Fig. 5K).

To explore whether AA supplementation can restore the effect of host defense in F0 EGCG-exposed females, we transferred the flies to the normal yeast-based diet with extra 10 mM of single AA including valine, leucine, isoleucine, phenylalanine, methionine, or tyrosine (Fig. 6A). After 3 days of administration, interestingly, leucine and methionine supplementation enhanced the resistance to *P. aeruginosa* infection compared to EGCG-exposed flies without extra supplementation (Fig. 6B). However, tyrosine supplementation eliminated the increasing survival rates of EGCG-exposed flies after infection (Fig. 6B). Furthermore, targeted metabolomics analysis showed that tyrosine supplementation restored the global levels of R5P, lactate, succinate, fumarate, malate, phenylalanine, cysteine, and glycine in the whole body (Fig. 6C).

Lactate functions as a heritable factor to mediate transgenerational host defense

Recent research has highlighted that the changes in maternal diet and metabolic defects in mothers can profoundly affect health and disease in their offspring [38]. To understand how EGCG-driven ATF4 activation could impact offspring epigenetic or metabolic reprogramming, we examined the metabolic changes that occur in the ovary. Consistent with our previous studies, several glycolysis-related intermediates were increased, indicating an enhance glycolytic activity (Fig. 7A). Additionally, we also observed an accumulation of nucleotide-related metabolite (R5P, E4P, and R5P), suggesting that PPP flux may also be increased (Fig. 7A). Among these increased metabolites, we noted a marked change in lactate (Fig. 7B), an important byproduct of glycolysis, with the greatest fold changes (2.23 higher than control group). As we previously described, the global level of lactate in the F0 flies were increased, while fat body and intestine remained unchanged (Fig. 3J and Fig. 5A). Taken together, we suppose that the total lactate accumulation in F0 flies is attributed to the increased lactate in the ovary. This provides insight into our previous reports. Notably, lactate has been implicated to function as a substrate for nuclear acetyl-CoA, thereby converting to H3K27ac [39]. Lactate is exported *via* monocarboxylate transporters (MCTs) and subsequently utilized as a metabolic fuel or signaling molecule in neighboring or distant cells [40]. We therefore propose that ovary-derived lactate could be delivered to the embryo and serve as a carbon source for H3K27ac in the F1 generation (Fig. 7C). In line with this hypothesis, we could not detect any changes of acetyl-CoA or histone acetylation (H3K9ac and H3K27ac) in the F0 ovary (Fig. 7, D and E), confirming that ovary-derived lactate failed to be utilized for acetylation in the tissue.

To demonstrate this model, we analyzed metabolites by GC–MS in F1 embryos collected 2–4 h after egg laying (Fig. 7F). The result showed a decreased level of lactate, while pyruvate and TCA intermediates including citrate, succinate and malate were increased, implying that lactate may fuel for TCA cycle and serve as a substrate for H3K27ac in the embryos of EGCG-exposed flies. In addition, sodium oxamate, an LDH inhibitor, was used to inhibit the lactate production in EGCG-exposed females. We treated 3- or 4-

Fig. 3. EGCG activates glycolysis to support anabolism. (A) Glucose metabolism pathway. Created with BioRender.com. (B and C) Relative mRNA levels of glycolysis-related genes in F0 (B) and F1 (C) flies. Ten flies were pooled for one individual. n = 3 biological replicates per group. (D and E) Glucose levels in F0 (D) and F1 (E) flies. About thirty flies were pooled for one individual. FW, fresh weight. n = 6 biological replicates per group. (F and G) Triglyceride levels in F0 (D) and F1 (E) flies. FW, fresh weight. n = 6 biological replicates per group. (H and I) PCA analysis (H) and heatmaps (I) of targeted metabolomics by GC–MS and LC-MS analysis in F0 and F1 flies. n = 6 biological replicates per group. (J and K) Relative amount of targeted metabolomics by GC–MS or LC-MS analysis in the fat body of F0 (J) and F1 (K) flies. n = 4 biological replicates per group. (L) ^{13}C-tracing experimental design. Created with BioRender.com. (M and N) Metabolic flux analysis in fat body (M) and whole body (N) from F0 and F1 flies. For fat body, about 20 fat bodies were dissected 24 h after ^{13}C-glucose labeling and pooled for one individual. n = 3 biological replicates per group. For whole body, five whole bodies were collected 48 h after ^{13}C-glucose labeling and pooled for one individual. n = 3 biological replicates per group. Statistical significance was calculated by two-tailed Student's t-tests. Error bars represent s.e.m. *P* values are depicted on the figures; $^{*}P < 0.05$; $^{**}P < 0.01$; $^{***}P < 0.001$; $^{****}P < 0.0001$. G6P, glucose 6-phosphate; F6P, fructose 6-phosphate; F16BP, fructose 1,6-bisphosphate; GAP, glyceraldehyde 3-phosphate; DHAP, dihydroxyacetone phosphate; G3P, glycerol 3-phosphate; 3PG, 3-phosphoglycerate; PEP, phosphoenolpyruvate; 2 KG, 2-ketoglutarate; R5P, ribose 5-phosphate; E4P, erythrose 4-phosphate; S7P, sedoheptulose 7-phosphate; SAM, S-adenosylmethionine; SAH, S-adenosylhomocysteine; ATP, adenosine triphosphate; ADP, adenosine diphosphate; AMP, adenosine monophosphate; $NADP^{+}$, nicotinamide adenine dinucleotide phosphate (oxidized form).

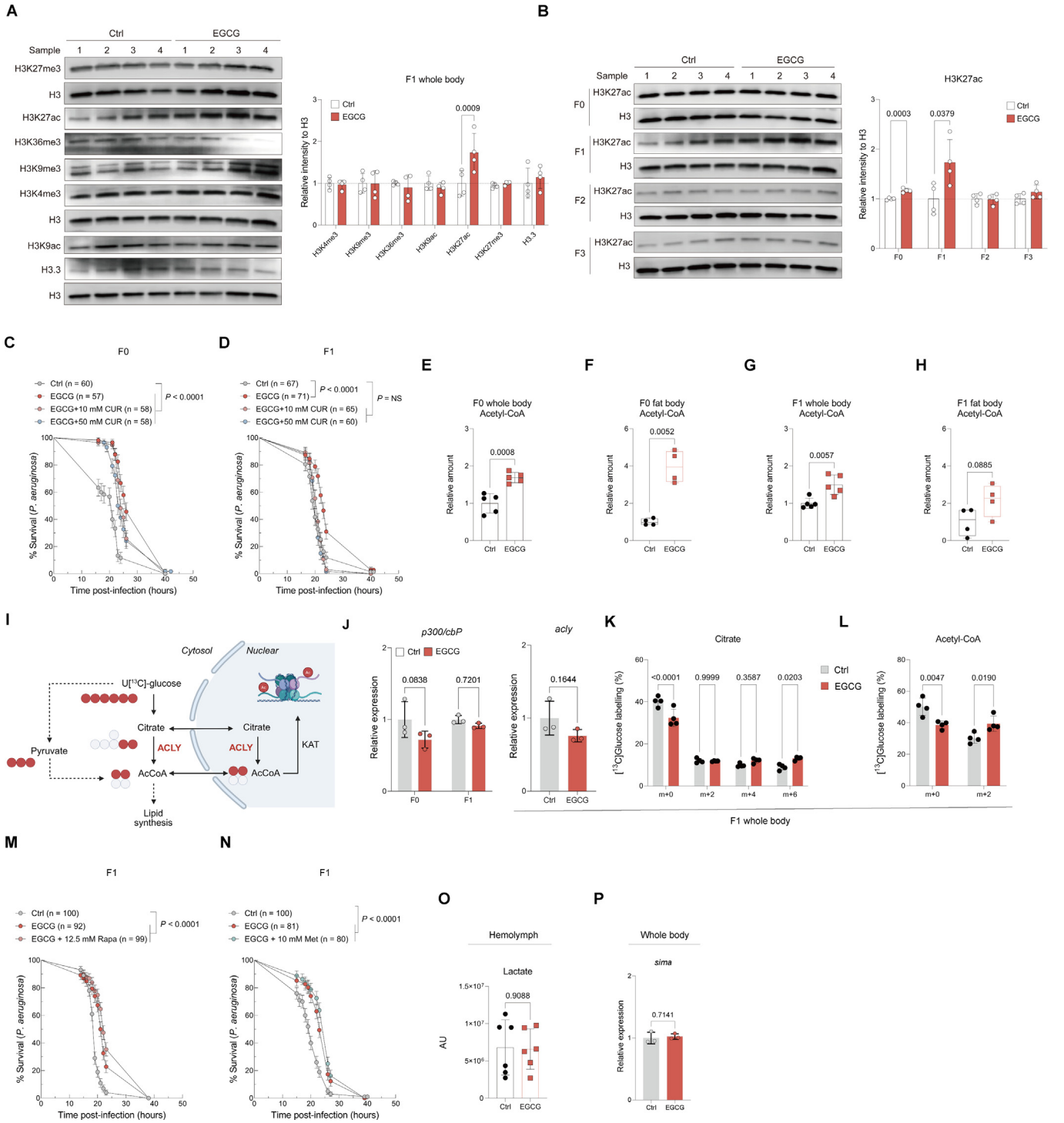

Fig. 4. H3K27ac correlates with the immune priming in offspring. (A) Western blot images and relative protein level of various histone modifications to histone H3 in F1 whole flies. H3K4me3, histone H3 lysine 4 trimethylation; H3K9me3, histone H3 lysine 9 trimethylation; H3K36me3, histone H3 lysine 36 trimethylation; H3K9ac, histone H3 lysine 9 acetylation; H3K27ac, histone H3 lysine 27 acetylation; H3K27me3, histone H3 lysine 27 trimethylation; H3.3, histone H3 variant. n = 4 biological replicates per group. (B) Western blot images and relative protein level of H3K27ac to histone H3 in F0, F1, F2, and F3 whole flies. n = 4 biological replicates per group. (C and D) Survivorship on F0 (C) and F1 (D) flies with 10 and 50 mM of curcumin administration for 3 days following *P. aeruginosa* infection. Sample sizes (n) are shown in the figure. (E and F) Relative amount of acetyl-CoA in whole body (E) and fat body (F) from F0 flies. For whole body or fat body, n = 4 ~ 5 biological replicates per group. (G and H) Relative amount of acetyl-CoA in whole body (G) and fat body (H) from F0 flies. For whole body or fat body, n = 4 ~ 5 biological replicates per group. (I) ^{13}C-glucose for stable isotope tracing experiments in F1 whole flies. AcCoA, acetyl-CoA. ACLY, ATP citrate lyase. KAT, lysine acetyltransferase. Created with BioRender.com. (J) Relative mRNA level of *p300/CBP* in F0 and F1 whole flies and *Acly* in F1 whole flies. n = 3 individuals per group. (K and L) Bar graphs show percent labeling of citrate (K) and acetyl-CoA (L) in F1 whole flies. Note, m + 2 and m + 4 are the labeling fractions of citrate derived from ^{13}C-glucose, and m + 2 is the labeling fraction of acetyl-CoA derived from ^{13}C-glucose. n = 3 biological replicates per group. (M and N) Survivorship on F1 flies with 12.5 mM rapamycin (M) and 10 mM metformin (N) administration for 3 days following *P. aeruginosa* infection. Rapa, rapamycin; Met, metformin. Sample sizes (n) are shown in the figure. (O) Relative peak area of circulating lactate in F1 hemolymph 3 h after *P. aeruginosa* infection. Ten flies were pooled for one individual. n = 6 biological replicates per group. AU, arbitrary unit. (P) Relative mRNA expression of *sima* in F1 whole flies 3 h after *P. aeruginosa* infection. n = 3 biological replicates per group. For survivorship, statistical significance was calculated by the log-rank test. For statistical analyses between two samples, two-tailed Student's t-tests were used. Error bars represent s.e.m. *P* values are depicted on the figures; $^{*}P < 0.05$; $^{**}P < 0.01$; $^{***}P < 0.001$; $^{****}P < 0.0001$; NS, not significance.

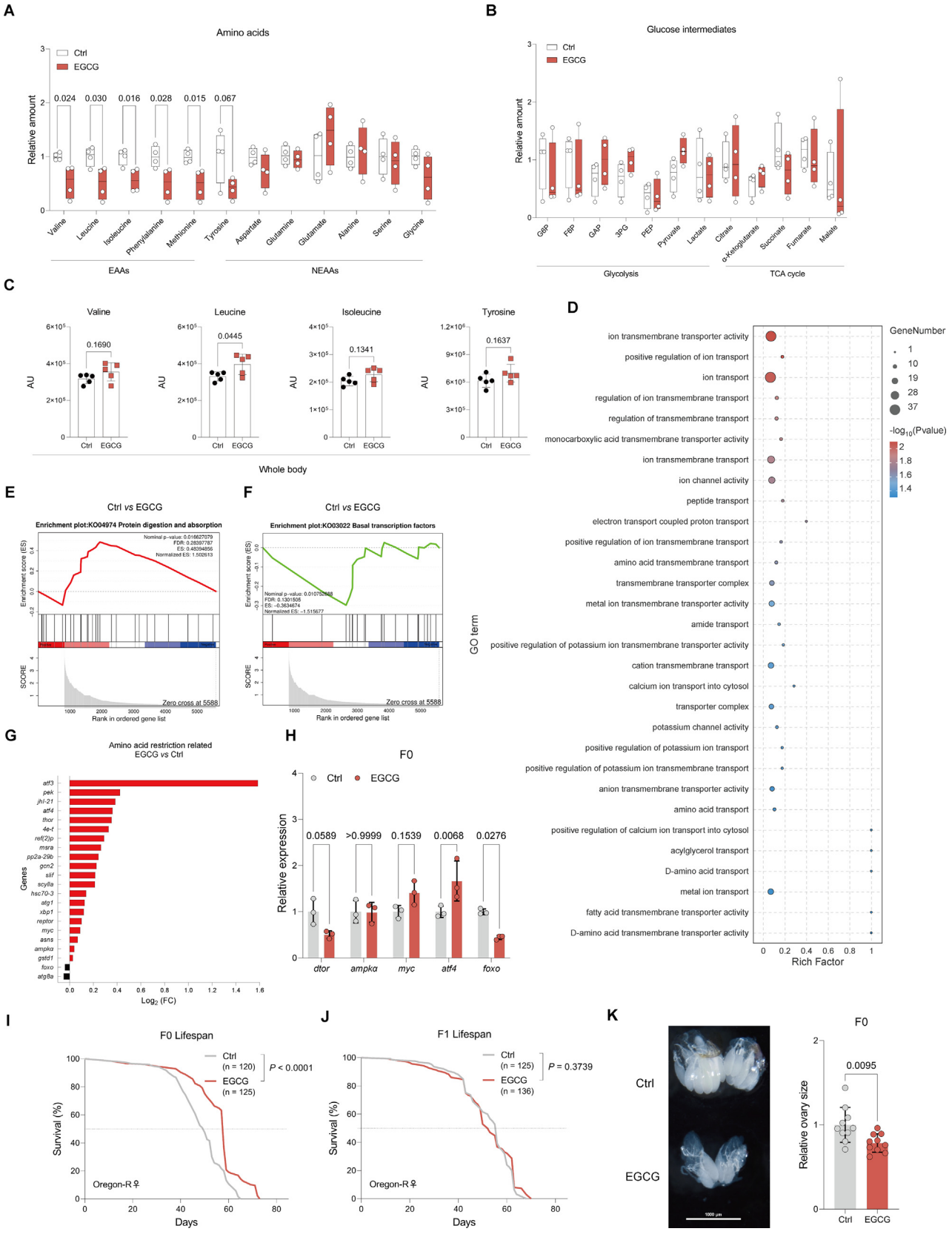
A
Amino acids
Ctrl
EGCG
Relative amount
0.024 0.030 0.016 0.028 0.015 0.067
Valine Leucine Isoleucine Phenylalanine Methionine Tyrosine Aspartate Glutamine Glutamate Alanine Serine Glycine
EAAs
NEAAs
B
Glucose intermediates
Ctrl
EGCG
Relative amount
G6P F6P GAP 3PG PEP Pyruvate Lactate Citrate α-Ketoglutarate Succinate Fumarate Malate
Glycolysis
TCA cycle
C
Valine
Leucine
Isoleucine
Tyrosine
AU
0.1690
0.0445
0.1341
0.1637
Ctrl EGCG
Whole body
D
ion transmembrane transporter activity
positive regulation of ion transport
ion transport
regulation of ion transmembrane transport
regulation of transmembrane transport
monocarboxylic acid transmembrane transporter activity
ion transmembrane transport
ion channel activity
peptide transport
electron transport coupled proton transport
positive regulation of ion transmembrane transport
amino acid transmembrane transport
transmembrane transporter complex
metal ion transmembrane transporter activity
amide transport
positive regulation of potassium ion transmembrane transporter activity
cation transmembrane transport
calcium ion transport into cytosol
transporter complex
potassium channel activity
positive regulation of potassium ion transport
positive regulation of potassium ion transmembrane transport
anion transmembrane transporter activity
amino acid transport
positive regulation of calcium ion transport into cytosol
acylglycerol transport
D-amino acid transport
metal ion transport
fatty acid transmembrane transporter activity
D-amino acid transmembrane transporter activity
GO term
Rich Factor
GeneNumber
1
10
19
28
37
-log10(Pvalue)
2
1.8
1.6
1.4
E
Ctrl vs EGCG
Enrichment plot:KO04974 Protein digestion and absorption
Enrichment score (ES)
SCORE
Zero cross at 5588
Rank in ordered gene list
F
Ctrl vs EGCG
Enrichment plot:KO03022 Basal transcription factors
Enrichment score (ES)
SCORE
Zero cross at 5588
Rank in ordered gene list
G
Amino acid restriction related
EGCG vs Ctrl
Genes
atf3 pek jhl-21 atf4 thor 4e-t ref(2)p msra pp2a-29b gcn2 slif scylla hsc70-3 atg1 xbp1 reptor myc asns ampka gstd1 foxo atg8a
Log2 (FC)
H
F0
Ctrl
EGCG
Relative expression
0.0589 >0.9999 0.1539 0.0068 0.0276
dtor ampka myc atf4 foxo
I
F0 Lifespan
Ctrl (n = 120)
EGCG (n = 125)
P < 0.0001
Survival (%)
Oregon-R♀
Days
J
F1 Lifespan
Ctrl (n = 125)
EGCG (n = 136)
P = 0.3739
Survival (%)
Oregon-R♀
Days
K
Ctrl
EGCG
F0
0.0095
Relative ovary size
Ctrl EGCG

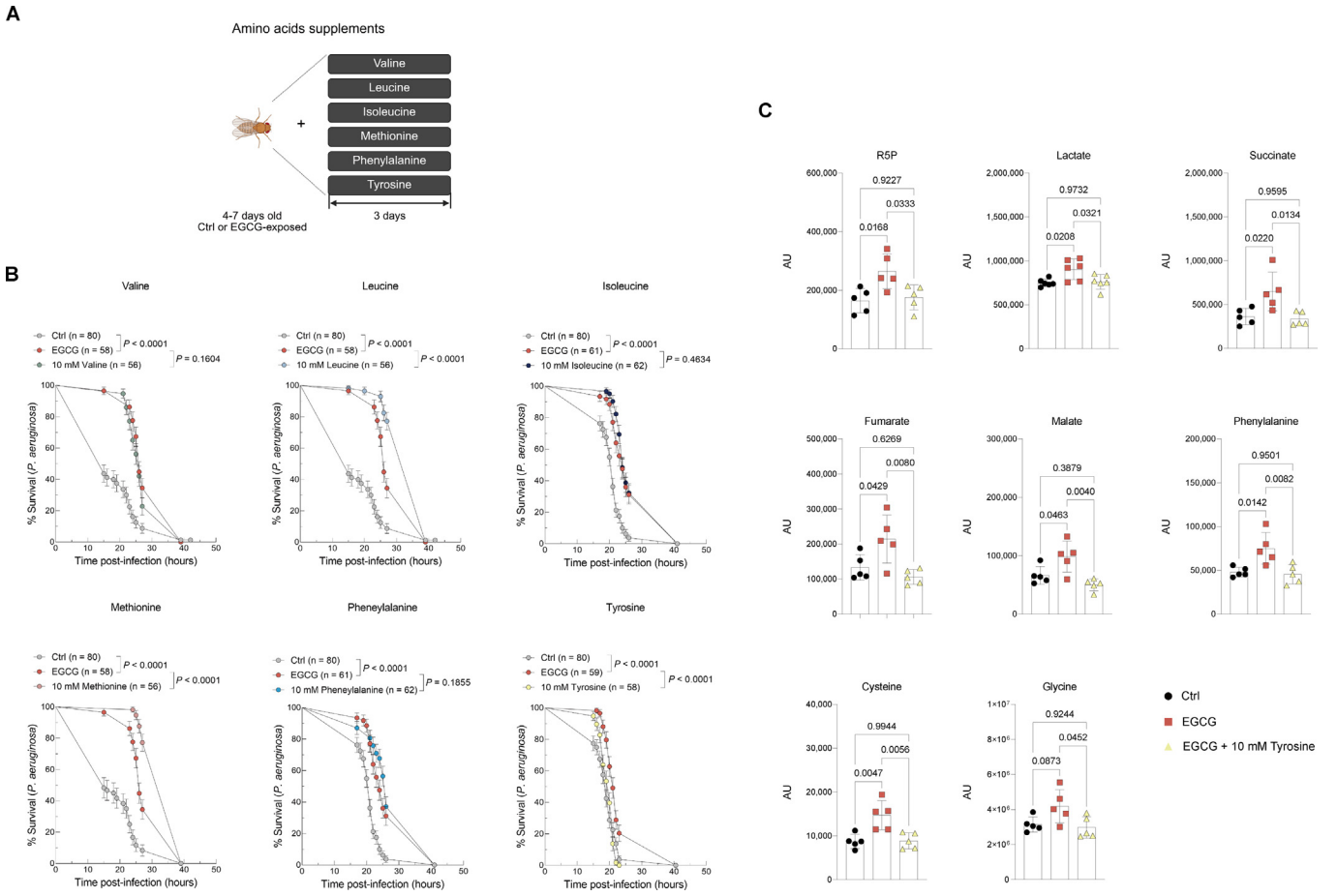

Fig. 6. Dietary tyrosine supplementation abolishes parental host defense and metabolic changes. (A) Experimental design. Created with BioRender.com. (B) Survivorship on F0 flies with 10 mM of valine, leucine, isoleucine, methionine, phenylalanine, and tyrosine administration for three days following *P. aeruginosa* infection. Sample sizes (n) are shown in the figure. (C) Altered metabolites in F0 flies with 10 mM of tyrosine administration for three days. n = 5 ~ 6 biological replicates per group. For statistical analyses between two samples, two-tailed Student's t-tests were used. For statistical analyses among three samples, one-way ANOVA tests were used. Error bars represent s.e.m. *P* values are depicted on the figures; $^{*}P < 0.05$; $^{**}P < 0.01$; $^{***}P < 0.001$; $^{****}P < 0.0001$.

day-old F0 EGCG-exposed flies with 10 or 50 mM of sodium oxamate for 3 days and subsequently generated the F1 females as previously described (Fig. 7G). Treatment with 50 mM sodium oxamate decreased the survival following *P. aeruginosa* infection and reduced the level of H3K27ac in EGCG-F1 flies (Fig. 7, H and I).

Discussion

In this study, we identify a previously unrecognized link between dietary EGCG, immunometabolic reprogramming, and transgenerational host defense. Our findings establish a model in which parental EGCG exposure induces a coordinated metabolic-epigenetic program that enhances resistance to bacterial infection and confers improved immune function to subsequent generations with non-genetic alteration (Fig. 8). Notably, we uncover a lactate-acetyl-CoA-H3K27ac axis as a central mechanistic link connecting metabolic remodeling to heritable immune protection.

EGCG exposure induces widespread metabolic remodeling across tissues in *Drosophila*. In particular, we observed an enhanced anabolic capacity and low energy turnover, which is similar to dietary restriction-induced metabolic response. This conversion may promote survival under environmental stress and support antimicrobial defense. Consistent with this, the reduction of intestinal AAs suggests a dietary restriction-associated metabolic adaptation, while dietary restriction is known to extend lifespan and enhance pathogen resistance [41]. In response to dietary restriction, autophagy is activated to recycle intracellular components, thereby releasing basic metabolic units such as amino acids

Fig. 5. EGCG-triggered integrated stress response correlates with parental metabolic rewiring. (A and B) Relative amounts of amino acids (A) and glucose intermediates (B) in the intestine of F0 flies. EAAs, essential amino acids. NEAAs, non-essential amino acids. G6P, glucose 6-phosphate; F6P, fructose 6-phosphate; GAP, glyceraldehyde 3-phosphate. 3PG, 3-phosphoglycerate; PEP, phosphoenolpyruvate; n = 3 biological replicates per group. (C) Relative peak area of valine, leucine, isoleucine, and tyrosine in F0 whole flies. AU, arbitrary unit. n = 5 biological replicates per group. (D) GO enrichment analysis of differentially expressed genes in F0 whole flies. The bubble plot displays the top 30 significantly enriched transport-related GO terms. The x-axis represents the rich factor, bubble size indicates the number of genes, and color reflects the adjusted P-value. (E and F) Gene Set Enrichment Analysis (GSEA) enrichment plots for the Protein digestion and absorption (E) and Basal transcription factors (F) pathways in F0 whole flies. The enrichment score (ES), normalized enrichment score (NES), nominal *P*-value, and FDR q-value are shown in the figure. (G) Graph showing amino acid restriction involved genes that were regulated in F0 whole flies. Fold-change (FC) values are expressed s $\log_2$ (FC) values. (H) Relative mRNA levels of *dtor*, ampk*α*, *myc*, *atf4*, and *foxo* in F0 whole flies. n = 3 biological replicates per group. (I and J) Lifespan of F0 (I) and F1 (J) flies. Sample sizes (n) are shown in the figure. (K) Representative images of the ovaries and the quantification of ovary sizes from F0 flies. Scale bars, 1 mm. n = 10 ovaries per group. For statistical analyses between two samples, two-tailed Student's t-tests were used. Error bars represent S.E.M. *P* values are depicted on the figures; $^{*}P < 0.05$; $^{**}P < 0.01$; $^{***}P < 0.001$; $^{****}P < 0.0001$.

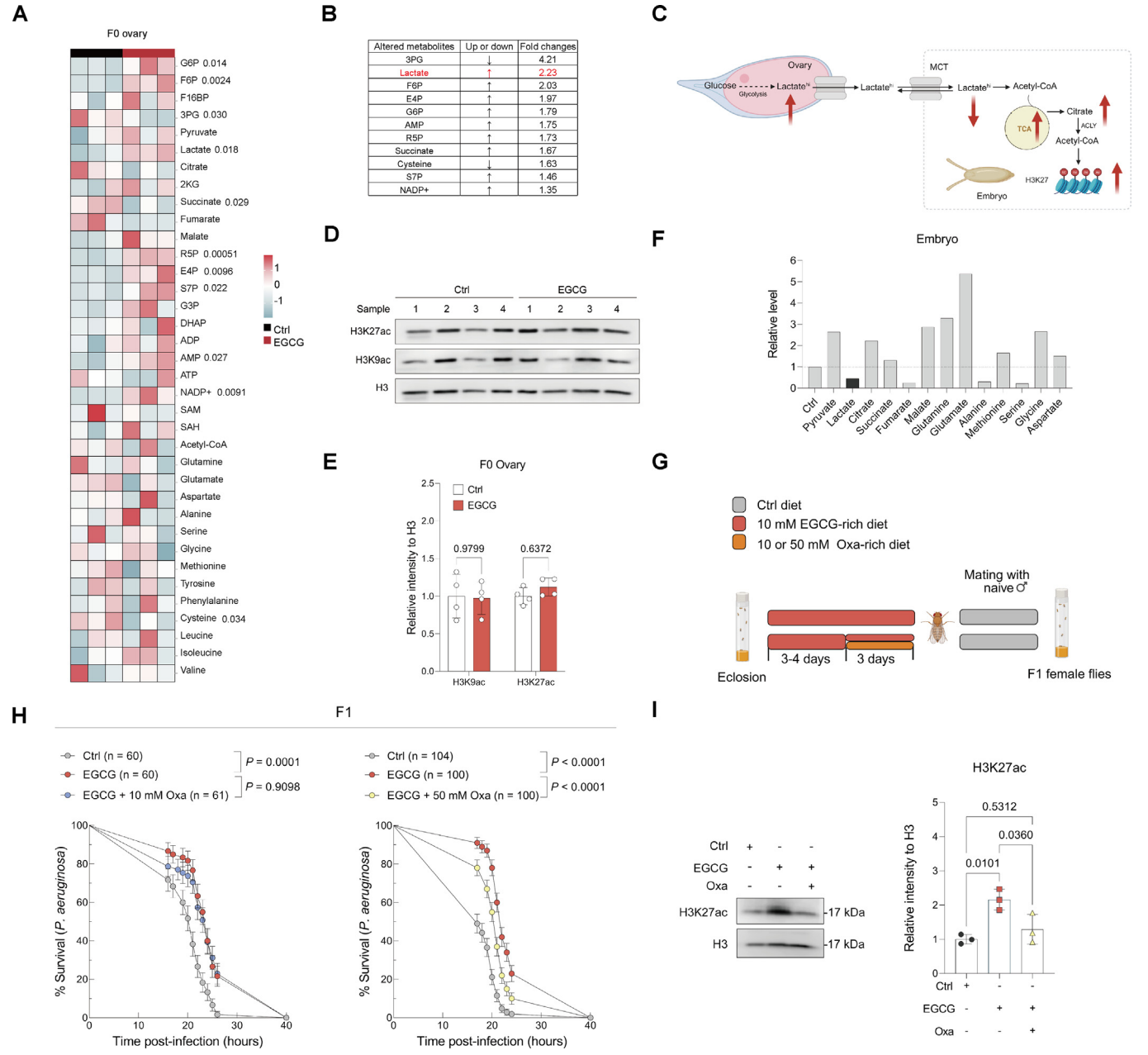

Fig. 7. Lactate functions as a heritable factor to mediate transgenerational host defense. (A and B) A heatmap (A) and differential metabolites (B) of targeted metabolomics by GC–MS and LC-MS analysis in the ovary of F0 flies. n = 3 biological replicates per group. (C) Graph depicting elevated H3K27ac levels mediated by lactate. Created with BioRender.com. MCT, monocarboxylate transporter; ACLY, ATP citrate lyase. (D and E) Western blot images (D) and relative protein level (E) of H3K9ac and H3K27ac to histone H3 in the ovary of F0 flies. n = 4 biological replicates per group. (F) Relative metabolite levels in F1 embryos at 2–4 h after egg laying. (G) Experimental design. Created with BioRender.com. (H) Survivorship on F1 flies with 10 or 50 mM of sodium oxamate administration for 3 days following *P. aeruginosa* infection. Sample sizes (n) are shown in the figure. (I) Representative Western blot images and relative protein level of H3K27ac to histone H3 in the F1 flies. Oxa, 50 mM of sodium oxamate. n = 3 biological replicates per group. For survivorship, statistical significance was calculated by the log-rank test. For statistical analyses between two samples, two-tailed Student's t-tests were used. For statistical analyses among three samples, one-way ANOVA tests were used. Error bars represent s.e.m. *P* values are depicted on the figures; $^{*}P < 0.05$; $^{**}P < 0.01$; $^{***}P < 0.001$; $^{****}P < 0.0001$. G6P, glucose 6-phosphate; F6P, fructose 6-phosphate; F16BP, fructose 1,6-bisphosphate; GAP, glyceraldehyde 3-phosphate; DHAP, dihydroxyacetone phosphate; G3P, glycerol 3-phosphate; 3PG, 3-phosphoglycerate; PEP, phosphoenolpyruvate; 2 KG, 2-ketoglutarate; R5P, ribose 5-phosphate; E4P, erythrose 4-phosphate; S7P, sedoheptulose 7-phosphate; SAM, S-adenosylmethionine; SAH, S-adenosylhomocysteine; ATP, adenosine triphosphate; ADP, adenosine diphosphate; AMP, adenosine monophosphate; $NADP^{+}$, nicotinamide adenine dinucleotide phosphate (oxidized form).

and fatty acids [34]. This may partly explain the increased abundance of certain amino acids at the organismal level.

AA limitation is a well-established trigger of the ISR, leading to ATF4 activation [42]. Consistent with our results, dietary deprivation of tyrosine has been reported to prolong the lifespan and elicits adaptive responses through GCN2-independent ATF4 activation in *Drosophila* [18]. Given our previous observation that EGCG can non-enzymatically react with amino acids [32], we speculate that direct depletion of amino acids contributes to ISR activation. However, because ATF4 also regulates amino acid transport such as SLC38A2 and SLC7A5 and metabolic adaptation [43], we cannot exclude the possibility that the altered intestinal amino acid profile also reflects a secondary adaptive response downstream of ATF4 activation. Thus, the relationship between amino acid reduction and ATF4 signaling may involve both upstream triggering and feedback regulation.

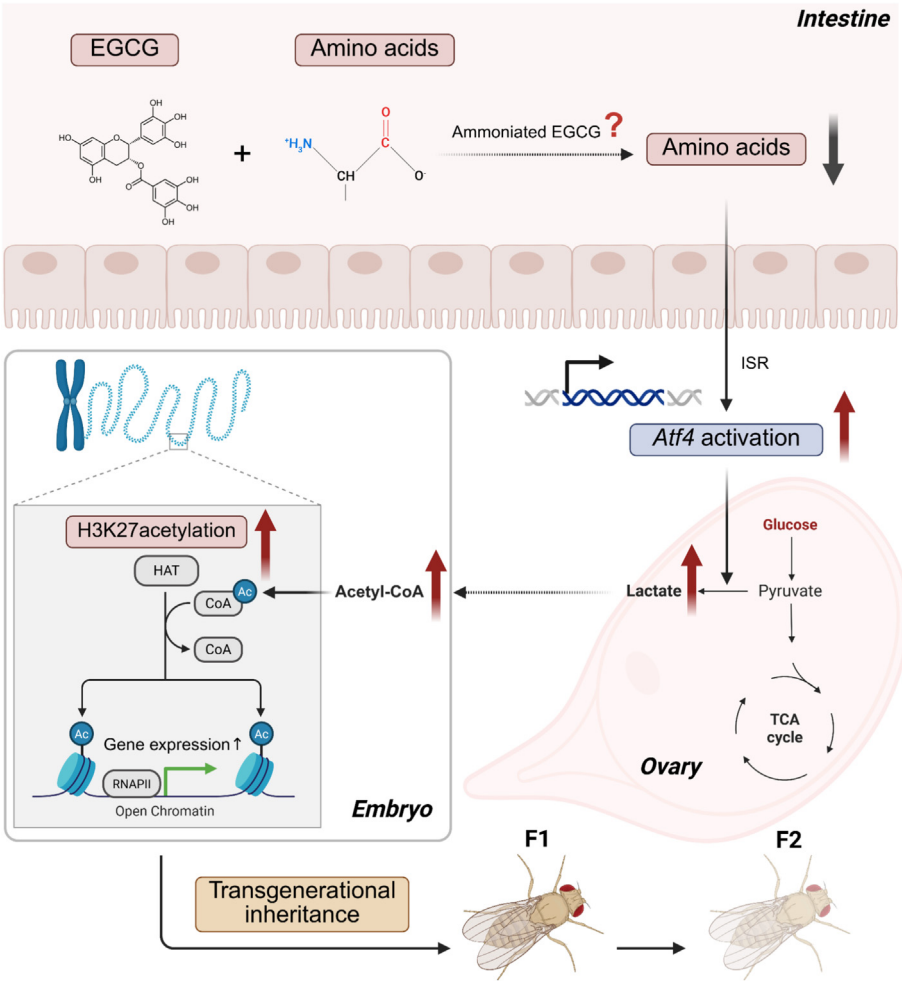

Fig. 8. Schematic model of EGCG-driven transgenerational inheritance *via* metabolic-epigenetic interplay in *Drosophila melanogaster*. EGCG may react with intestinal amino acids to reduce its bioavailability, leading to activation of the integrated stress response (ISR) and its downstream effector activating transcription factor 4 (ATF4). ATF4 activation promotes lactate production and accumulation in the ovary, which is subsequently transmitted to the next generation and contributes to increased acetyl-CoA availability and elevated H3K27ac levels in adult offspring. Created with BioRender.com.

ATF4 activation has been implicated in coordinating immunometabolic responses. In RAW264.7 cell lines, *Atf4* knockdown could partially block LPS-induced pro-inflammatory cytokines, lactate accumulation and glycolytic capacity [44]. Notably, ATF4 activation was recently shown to induce one-carbon metabolism in host mitochondria and use much more folate, hereby restricting parasite replication [45]. Our results support a role for ATF4 in mediating diet-induced transgenerational effects. Moreover, emerging evidence has demonstrated that yolk-based transport of histones coordinates the transmission of epigenetic modification between somatic tissues and germline cells [46]. ATF4 promotes yolk lipoprotein secretion from the fat body, which may imply that ATF4 is a key metabolic sensor mediating diet-induced transgenerational effects [47].

A central finding of this study is that lactate-derived acetyl-CoA serves as a metabolic-epigenetic bridge linking parental metabolic state to offspring chromatin regulation. Acetyl-CoA is the sole donor of histone acetylation, and the nuclear acetyl-CoA metabolism displays an important role in cellular metabolism and gene expression [5]. Many studies have emphasized that lactate can function as an intercellular signal to communicate with different cell types based on the theory of lactate shuttling [40]. For instance, the production of lactate increased in fibroblasts, and MCT1, which induces the influx of lactate, migrated to the myocardial membrane in a coculture system [48]. Our data support a model in which ovarian lactate functions as a maternal metabolic determinant for transgenerational inheritance. Notably, although lactate accumulates in the F0 ovary, acetyl-CoA and H3K27ac are not increased in this tissue, suggesting that lactate may contribute to metabolic-epigenetic regulation. By contrast, the reduction of lactate and the increase of TCA cycle intermediates in embryos suggest that maternal lactate may be deposited into the oocyte or early embryo and subsequently utilized as a carbon source to support acetyl-CoA production and H3K27ac establishment. We cannot, however, exclude an indirect mechanism whereby elevated ovarian lactate reprograms the metabolic state of the oocyte or other maternal signals that influence embryonic metabolism. Defining the precise route of lactate transfer from ovary to embryo will require future metabolic tracing studies.

Notably, lactate can also serve as a substrate for histone lactylation [40,49]. Although our study primarily supports a mechanism in which lactate promotes H3K27ac via conversion to acetyl-CoA, the elevated lactate levels observed in F0 and F1 flies, together with reports of histone lactylation during *Drosophila* gametogenesis [50], raise the possibility that lactylation may also be involved. Future studies are needed to determine whether EGCG induces histone lactylation and whether it acts in concert with H3K27ac in transgenerational immune regulation.

The sex-specific nature of the host-defense phenotype likely reflects the interaction between transmitted parental signals and the sex-specific physiological context of the offspring, rather than a single uniform mechanism. Previous studies have shown that intergenerational and transgenerational responses are frequently sex biased, with contributions from sex chromosomes, endocrine regulation, and germline-specific epigenetic carriers. In mammals, X-linked dosage, Y-linked modifiers, and sex hormone signaling can reshape metabolic and immune transcriptional programs through epigenetic remodeling, thereby altering how inherited signals are interpreted in male and female offspring [51,52]. In parallel, the paternal and maternal germlines differ fundamentally in the types of information they deliver to the zygote: sperm mainly transmit chromatin-associated information and small non-coding RNAs, whereas oocytes additionally provide abundant cytoplasmic metabolites, maternal RNAs, and organelles [53,54]. These differences may help explain why a related metabolic perturbation can produce sex-dependent outcomes and distinct inheritance patterns across species. In our study, our data are most consistent with a model in which maternal deposition-mediated metabolic-epigenetic remodeling plays a major role in shaping the inherited phenotype.

The difference in the number of transmitted generations observed between mice and *Drosophila* may reflect both experimental design and biological divergence. In particular, embryonic exposure in *Drosophila* may allow direct metabolic and epigenetic programming of early developmental stages, thereby facilitating transmission to subsequent generations. In contrast, adult exposure in mammals may primarily influence mature somatic-germline communication, resulting in more limited intergenerational effects. At the same time, fundamental differences in epigenetic reprogramming between mammals and invertebrates may further contribute to these distinct inheritance patterns.

EGCG is a common dietary compound and well-known for several health effects *i.e.*, antioxidant, anti-inflammatory and anti-cancer properties [55–57]. In different models, multiple pathways including the modulation of sirtuins [58], the AMPK/mTOR pathway [9], and NF-κB [59] have been proposed to exert the immunomodulatory effects. Given the pharmacological diversity of natural products, it is challenging to attribute a single phenotypic effect to a specific mechanism. These properties may also affect EGCG-induced bacterial protection and metabolic-epigenetic interplay. For instance, EGCG was found to inhibit biofilm production in *S. aureus* [60]. However, our study suggests that EGCG-induced bacterial protection cannot be fully explained by its direct antimicrobial or classic immunomodulatory effects. Instead, EGCG acts as a dietary signal that reprograms host immunometabolic and epigenetic states, resulting in sustained and heritable immune protection.

From a translational perspective, body surface area normalization suggests that the dose used in mice corresponds to a human equivalent of approximately 1.5–1.7 g/day. Although this exceeds typical dietary intake from green tea, it falls within the range used in supplementation and pharmacological studies. Therefore, these findings should be interpreted as a proof-of-concept mechanism rather than a direct recommendation for high-dose EGCG intake, providing a conceptual framework for how dietary polyphenols may influence offspring health.

Conclusion

In conclusion, our findings demonstrate that specific dietary components have the potential to improve immune health across generations and provide an intriguing new model for how dietary factor substances can induce the transgenerational inheritance of host defense. By linking amino acid sensing, ATF4 activation and lactate-derived acetyl-CoA metabolism, we provide mechanistic insight into how dietary cues are translated into sustained and heritable host defense. These results highlight metabolic-epigenetic interplay as a fundamental principle underlying immune adaptation and its transmission across generations. Importantly, whether ATF4-driven metabolic remodeling actively shapes heritable epigenetic states, and how such information is transmitted from somatic tissues to the germline, remains to be explored. Besides H3K27 acetylation, other epigenetic modifications such as non-coding RNAs and RNA methylation may also contribute to diet-induced transgenerational immune effects.

Declaration of competing interest

The authors declare that they have no known competing financial interests or personal relationships that could have appeared to influence the work reported in this paper.

Acknowledgements

This work was supported by National Natural Science Foundation of China (32472327), the Ramón y Cajal grant (RYC2020-030365-I to Jianbo Xiao), the Xunta de Galicia "Excelencia" program (ED431F2022/01 to Jianbo Xiao) and the Juan de la Cierva Incorporación grant (IJC2020-046055-I to Hui Cao). Funding for open access charge was provided by the University of Vigo/CISUG.

Appendix A. Supplementary data

Supplementary data to this article can be found online at https://doi.org/10.1016/j.jare.2026.04.028.

References

[1] Domínguez-Andrés J et al. Trained immunity: adaptation within innate immune mechanisms. Physiol Rev 2022.
[2] Tetreau G et al. Trans-generational immune priming in invertebrates: current knowledge and future prospects. Front Immunol 2019;10:1938.
[3] Roth O et al. Recent advances in vertebrate and invertebrate transgenerational immunity in the light of ecology and evolution. Heredity 2018;121(3):225–38.
[4] Lee JE et al. Acute dietary restriction acts via TOR, PP2A, and Myc signaling to boost innate immunity in Drosophila. Cell Rep 2017;20(2):479–90.
[5] Boon R, Silveira GG, Mostoslavsky R. Nuclear metabolism and the regulation of the epigenome. Nat Metab 2020;2(11):1190–203.
[6] Barge SR et al. A traditional fermented bamboo shoot reduces intracellular fat accumulation and promotes fat browning in differentiated 3T3-L1 adipocyte cells through the activation of the AMPK signaling pathway. Food Front 2024;5(4):1642–57.
[7] Rangsinth P et al. *Amauroderma rugosum* extract improves brain function in d-galactose-induced aging mouse models via the regulatory effects of its polysaccharides on oxidation, the mTOR-dependent pathway, and gut microbiota. Food Front 2025;6(2):872–90.
[8] Biswas S et al. Role of nutraceuticals in viral infections as immunomodulators: a comprehensive review. eFood 2024;5(5):e70000.
[9] Holczer M et al. Epigallocatechin-3-gallate (EGCG) promotes autophagy-dependent survival via influencing the balance of mTOR-AMPK pathways upon endoplasmic reticulum stress. Oxidative Med Cell Longev 2018;2018:15.
[10] Xiao X et al. Unraveling the superiority of (−)-gallocatechin gallate to (−)-epigallocatechin-3-gallate in protection of diabetic nephropathy of db/db mice. Food Front 2024;5(2):771–88.
[11] Khan H et al. Targeting epigenetics in cancer: therapeutic potential of flavonoids. Crit Rev Food Sci Nutr 2021;61(10):1616–39.
[12] Zhang SS et al. Epigallocatechin-3-gallate (EGCG) inhibits imiquimod-induced psoriasis-like inflammation of BALB/c mice. BMC Complement Altern Med 2016;16:11.
[13] Isbrucker RA et al. Safety studies on epigallocatechin gallate (EGCG) preparations. Part 1: genotoxicity. Food Chem Toxicol 2006;44(5):626–35.
[14] Lambert JD et al. Hepatotoxicity of high oral dose (-)-epigallocatechin-3-gallate in mice. Food Chem Toxicol 2010;48(1):409–16.
[15] Zheng X et al. Intergenerational inheritance of quercetin-induced abnormal immunity in mice. Crit Rev Food Sci Nutr 2025:1–12.
[16] Chen PB et al. Epigallocatechin gallate (EGCG) alters body fat and lean mass through sex-dependent metabolic mechanisms in *Drosophila melanogaster*. Int J Food Sci Nutr 2019;70(8):959–69.

[17] Wagner AE et al. Epigallocatechin gallate affects glucose metabolism and increases fitness and lifespan in *Drosophila melanogaster*. Oncotarget 2015;6 (31):30568–78.
[18] Kosakamoto H et al. Sensing of the non-essential amino acid tyrosine governs the response to protein restriction in Drosophila. Nat Metab 2022;4(7):944.
[19] Neyen C et al. Methods to study Drosophila immunity. Methods 2014;68 (1):116–28.
[20] Wang RH et al. Global stable-isotope tracing metabolomics reveals system-wide metabolic alternations in aging Drosophila. Nat Commun 2022;13(1):14.
[21] Millard P et al. IsoCor: correcting MS data in isotope labeling experiments. Bioinformatics 2012;28(9):1294–6.
[22] Krejčová G et al. Drosophila macrophages switch to aerobic glycolysis to mount effective antibacterial defense. eLife 2019;8:e50414.
[23] Hancock REW, Nijnik A, Philpott DJ. Modulating immunity as a therapy for bacterial infections. Nat Rev Microbiol 2012;10(4):243–54.
[24] Bird L. Getting enough energy for immunity. Nat Rev Immunol 2019;19 (5):269.
[25] Tucey TM et al. Glucose homeostasis is important for immune cell viability during candida challenge and host survival of systemic fungal infection. Cell Metab 2018;27(5):988.
[26] Bharucha KN. The epicurean fly: using drosophila melanogaster to study metabolism. Pediatr Res 2009;65(2):132–7.
[27] Buchon N, Silverman N, Cherry S. Immunity in Drosophila melanogaster - from microbial recognition to whole-organism physiology. Nat Rev Immunol 2014;14(12):796–810.
[28] DeBerardinis RJ, Chandel NS. We need to talk about the Warburg effect. Nat Metab 2020;2(2):127–9.
[29] Wan QL et al. Histone H3K4me3 modification is a transgenerational epigenetic signal for lipid metabolism in *Caenorhabditis elegans*. Nat Commun 2022;13 (1):14.
[30] Cheng SC et al. mTOR- and HIF-1α-mediated aerobic glycolysis as metabolic basis for trained immunity. Science 2014;345(6204):1579.
[31] Balasubramanyam K et al. Curcumin, a novel p300/CREB-binding protein-specific inhibitor of acetyltransferase, represses the acetylation of histone/nonhistone proteins and histone acetyltransferase-dependent chromatin transcription. J Biol Chem 2004;279(49):51163–71.
[32] Zhang H et al. Ammoniation of dietary flavonoids containing a pyrogallol group with amino acids at 37° C. Food Chem Int 2025;1(1):44–60.
[33] Zhang H et al. Amination of flavonoids possessing a pyrogallol group in cell culture medium at 37° C. Food Front 2025;6(2):1058–78.
[34] Long H, Panda S. Time-restricted feeding and circadian autophagy for long life. Nat Rev Endocrinol 2022;18(1):5–6.
[35] Pakos-Zebrucka K et al. The integrated stress response. EMBO Rep 2016;17 (10):1374–95.
[36] Sorge S et al. ATF4-induced Warburg metabolism drives over-proliferation in Drosophila. Cell Rep 2020;31(7):20.
[37] Kosakamoto H et al. Context-dependent impact of the dietary non-essential amino acid tyrosine on Drosophila physiology and longevity. Sci Adv 2024;10 (35):13.
[38] Hocaoglu H et al. Heritable shifts in redox metabolites during mitochondrial quiescence reprogramme progeny metabolism. Nat Metab 2021;3(9):1259.
[39] Shi WW et al. Lactic acid induces transcriptional repression of macrophage inflammatory response via histone acetylation. Cell Rep 2024;43(2):24.
[40] Li XL et al. Lactate metabolism in human health and disease. Signal Transduct Target Ther 2022;7(1):22.
[41] Palma C et al. Caloric restriction promotes immunometabolic reprogramming leading to protection from tuberculosis. Cell Metab 2021;33(2):300.
[42] Efeyan A, Comb WC, Sabatini DM. Nutrient-sensing mechanisms and pathways. Nature 2015;517(7534):302–10.
[43] Yan X, Liu CH. The ATF4-glutamine axis: a central node in cancer metabolism, stress adaptation, and therapeutic targeting. Cell Death Discov 2025;11(1):11.
[44] Liu TT et al. ATF4 knockdown in macrophage impairs glycolysis and mediates immune tolerance by targeting HK2 and HIF-1α ubiquitination in sepsis. Clin Immunol 2023;254:16.
[45] Medeiros TC et al. Mitochondria protect against an intracellular pathogen by restricting access to folate. Science 2025;389(6761):eadr6326.
[46] Zhang QH, Dang WW, Wang MC. Lysosomes signal through the epigenome to regulate longevity across generations. Science 2025;389(6767):1353–60.
[47] Grmai L et al. Integrated stress response signaling acts as a metabolic sensor in fat tissues to regulate oocyte maturation and ovulation. Cell Rep 2024;43 (3):20.
[48] Brooks GA. Lactate shuttles in nature. Biochem Soc Trans 2002;30:258–64.
[49] Zhang D et al. Metabolic regulation of gene expression by histone lactylation. Nature 2019;574(7779):575.
[50] Hayashi Y et al. Comprehensive observation of histone lysine lactylation during gametogenesis of *Drosophila melanogaster*. Dev Dyn 2025:13.
[51] Shepherd R et al. Sexual dimorphism in innate immunity: the role of sex hormones and epigenetics. Front Immunol 2021;11:16.
[52] Dunn GA, Morgan CP, Bale TL. Sex-specificity in transgenerational epigenetic programming. Horm Behav 2011;59(3):290–5.
[53] Ben Maamar M, Nilsson EE, Skinner MK. Epigenetic transgenerational inheritance, gametogenesis and germline development. Biol Reprod 2021;105(3):570–92.
[54] Lismer A, Kimmins S. Emerging evidence that the mammalian sperm epigenome serves as a template for embryo development. Nat Commun 2023;14(1):22.
[55] Nikoo M, Regenstein JM, Gavlighi HA. Antioxidant and antimicrobial activities of (-)-epigallocatechin-3-gallate (EGCG) and its potential to preserve the quality and safety of foods. Compr Rev Food Sci Food Saf 2018;17(3):732–53.
[56] Ajaz M et al. Anti-inflammatory effects of flavonoids in otitis media: a systematic review of pre-clinical evidence. Food Front 2025;6(6):2554–74.
[57] Tang S et al. Structural insights and biological activities of flavonoids: Implications for novel applications. Food Front 2025;6(1):218–47.
[58] Han DW et al. Preventive effects of epigallocatechin-3-O-gallate against replicative senescence associated with p53 acetylation in human dermal fibroblasts. Oxidative Med Cell Longev 2012;2012:13.
[59] Luo KW et al. EGCG inhibited bladder cancer SW780 cell proliferation and migration both *in vitro* and *in vivo* via down-regulation of NF-κB and MMP-9. J Nutr Biochem 2017;41:56–64.
[60] Das S et al. Antimicrobial potential of epigallocatechin-3-gallate (EGCG): a green tea polyphenol. J Biochem Pharmacol Res 2014;2(3):167–74.